ESTIMATING PRIMARY PRODUCTION IN COASTAL WATERS WITH REMOTE SENSING

A Thesis Submitted to the
Graduate School of Natural and Applied Sciences of
Dokuz Eylül University
In Partial Fulfillment of the Requirements for
the Degree of Doctor of Philosophy in Marine Sciences and Technology, Coastal Engineering Program

by
Esin ÜÇÜNCÜOĞLU

January, 2002
İZMİR

Ph.D. THESIS EXAMINATION RESULT FORM

We certify that we have read this thesis **"ESTIMATING PRIMARY PRODUCTION IN COASTAL WATERS WITH REMOTE SENSING"** completed by **ESİN ÜÇÜNCÜOĞLU** under supervision of **PROF.DR. ORHAN USLU** and that in our opinion it is fully adequate, in scope and in quality, as a thesis for the degree of Doctor of Philosophy.

Prof.Dr. Orhan USLU

Supervisor

Prof.Dr. Nilgün HARMANCIOĞLU

Jury Member
(Thesis Committee Member)

Yar.Doç.Dr. Erdem SAYIN

Jury Member
(Thesis Committee Member)

Prof.Dr. Baha BÜYÜKIŞIK

Jury Member

Doç.Dr. Şükrü BEŞİKTEPE

Jury Member

Approved by the
Graduate School of Natural and Applied Sciences

Prof.Dr. Cahit HELVACI
Director

To my family

ACKNOWLEDGEMENTS

I would like to tank to all of my colleagues and friends for their help and assistance that they have provided during this study but there are some special ones whom I would like to mention about their support specially. First of all, I would like to thank to my supervisor, Prof. Dr. Orhan Uslu, who trusted in me more than myself. I deeply appreciate Dr. Çetin Başöz who helped me patiently to construct a database in FOXPRO environment. I would particularly like to thank to Richard P. Stumpf who have provided suggestions via email and have sent his papers to me when I felt desperate. I would also like to thank to Assoc. Prof. Dr. Şükrü Beşiktepe and his colleagues who have prepared the Ocean Color Training Course of NATO/IOCCG at Institute of Marine Sciences in Erdemli during September, 2000, where I had the opportunity to discuss my research with the experts came from Australia, Canada and Russia and receive advice and suggestions which helped a lot. Finally, I would like to acknowledge the staff of IMST who has worked hard to collect and analyze the *in situ* data so that I could perform such a study.

Esin ÜÇÜNCÜOĞLU

ABSTRACT

Remote sensing of ocean color is based on the measurement of water-leaving radiance in visible part of the electromagnetic spectrum. The total signal detected by the satellite sensor is corrected for the atmospheric noise. Then the concentrations of phytoplankton pigments in the surface layers of the ocean can be derived by using empirical algorithms. The algorithms in use generally fail in coastal waters, which are optically complex due to the presence of other substances like suspended solids. There are efforts on the development of new algorithms and new sensors to infer concentrations of phytoplankton pigments in coastal waters.

The NOAA's Advanced Very High Resolution Radiometer (AVHRR) was designed for meteorological purposes, not for use as an ocean color sensor. The most successful use of AVHRR data in oceanography is the determination of sea surface temperature maps. Although it does not have the sensitivity in the red and near-infrared to examine open ocean waters (case-1 waters), its sensitivity is suitable to examine the patterns in water clarity at turbid estuaries (case-2 waters) (Stumpf, 1987, 1992, Stumpf & Frayer 1997, Stumpf & Pennock 1989, 1991, Stumpf & Tyler, 1988, Tyler & Stumpf, 1989, Stumpf *et al*, 1999, Woodruff *et al.*, 1999).

Eutrophication due to the supply of organic matter is one of the most important environmental problems of Izmir Bay. Monitoring the levels of chlorophyll - as an indicator for eutrophication – through remote sensing has substantial benefits for the management of eutrophication.

The objective of this study is to construct a model, which estimates the distribution of aquatic chlorophyll-a concentrations in the surface layers of the Izmir Bay with interpretations of remote sensing observations and calculation of primary production based on empirical algorithms. The dataset covers *in situ* measurements carried out in Izmir Bay for the period of 1996-1998 and corresponding AVHRR (NOAA-14) images. Stumpf's (1992) algorithm is used to remove atmospheric effects from the images and retrieve the water leaving reflectances. Then a model is constructed to calibrate those reflectances with the *in situ* chlorophyll-a and attenuation coefficient data. Finally an empirical model is applied to estimate primary production from the remotely retrieved chlorophyll-a data.

ÖZET

Deniz renginin uzaktan algılanması, elektromanyetik spektrumun görünür aralığında sudan gelen ışımanın ölçülmesi temeline dayanır. Uydu alıcısı tarafından algılanan toplam sinyaldeki atmosferik etkiler giderilmelidir. Daha sonra deniz yüzeyindeki klorofil-a konsantrasyonları, ampirik algoritmalar kullanılarak elde edilebilir. Bu algoritmalar, askıda katı madde gibi başka materyallerin de bulunması nedeniyle optik açıdan karmaşık olan kıyısal sularda genellikle iyi sonuç vermemektedir. Kıyısal sularda fitoplankton pigmentlerinin konsantrasyonlarını verebilecek yeni algoritmalar ve alıcıların geliştirilmesi üzerinde halen çalışmalar devam etmektedir.

AVHRR (Advanced Very High Resolution Radiometer), elektromanyetik spektrumun görünür, yakın kızılötesi ve termal kızılötesi bölümlerinde algılayan, geniş bant aralıklarına sahip, beş kanallı bir tarayıcıdır. Bu alıcı NOAA'nın (US National Oceanic and Atmospheric Administration / ABD Okyanus ve Atmosfer Milli İdaresi) uydularında taşınmaktadır. AVHRR, deniz rengini algılamak için değil, meteorolojik amaçlarla geliştirilmiştir. AVHRR verilerinin oşinografide en başarılı kullanım şekli deniz yüzeyi sıcaklıkları haritalarının üretilmesidir. Bu alıcının kırmızı ve yakın-kızılötesi kanalları, açık deniz sularının (tip-1 sular) incelenmesi konusunda yetkin olmamasına rağmen, duyarlılığı bulanık körfezlerdeki suların (tip-2 sular) optik özelliklerinin incelenebilmesi için uygundur (Stumpf, 1987, 1992, Stumpf & Frayer 1997, Stumpf & Pennock 1989, 1991, Stumpf & Tyler, 1988, Tyler & Stumpf, 1989, Stumpf *et al*, 1999, Woodruff *et al.*, 1999).

Organik madde girdileri yüzünden oluşan ötrofikasyon, İzmir Körfezi'nin en önemli çevresel sorunlarından bir tanesidir. Uzaktan algılama yoluyla – ötrofikasyonun indikatörü olarak – klorofil seviyelerinin izlenmesi, ötrofikasyonun yönetimi açısından önemli faydalar sağlıyacaktır.

Bu çalışmanın amacı, uzaktan algılama gözlemlerinin yorumlanarak, İzmir Körfezi'nin yüzey tabakalarında bulunan klorofil-a konsantrasyonlarının dağılımını tahmin edecek bir model oluşturulması ve amprik algoritmalar kullanılarak birincil üretkenliğin hesaplanmasıdır. Bu çalışmada 1996-1998 yılları arasında İzmir Körfezi'nde Büyükşehir Belediyesi'nin desteği ile Deniz Bilimleri ve Teknolojisi Enstitüsü tarafından yürütülen "Deniz Çalışmaları" kapsamında toplanan verilerle aynı tarihlerde alınan NOAA-14 görüntüleri kullanılmıştır. Stumpf'un (1992) algoritması uygulanarak atmosferik etkiler giderilmiş ve deniz yüzeyi yansıması haritaları çıkarılmıştır. Bulunan yansımaların denizden toplanan verilerle regresyonu yapılarak, yansımadan klorofil-a elde edecek bir model oluşturulmuştur. Son olarak da uzakdan algılanmış klorofil-a konsantrasyonundan, amprik modellerin yardımıyla birincil üretkenlik tahmin edilmiştir.

CONTENTS

Chapter Two

THE ADVANCED VERY HIGH RESOLUTION RADIOMETER

Chapter Three

MATERIALS AND METHODS FOR REMOTE SENSING OF SEA SURFACE REFLECTANCE IN IZMIR BAY

Chapter Six
DISCUSSION AND CONCLUSIONS

LIST OF TABLES

LIST OF FIGURES

CHAPTER ONE
INTRODUCTION

1. Introduction

Traditionally, observations of the marine environment have been carried out on an occasional basis by oceanographic cruises. The data have been obtained for restricted geographical areas and on an irregular temporal basis. In the last decades regular repetitive coverage of the global oceans has been achieved by the satellites, which provide enormous amounts of data as compared to conventional monitoring methods. The main problem of the satellite observation is that the data obtained is not direct measurements of bio-geo-chemical and physical parameters of the sea as in conventional methods using instruments on a ship or buoy. However, considerable amount of processing and interpretation is necessary before one can actually obtain oceanographic parameters from the satellite data.

Satellite scanners are designed to receive the electromagnetic radiation for information acquisition and record the brightness values at each X and Y location called simply a "picture element" or "pixel". Reducing the size or spacing of the grid finer spatial resolutions can be achieved. Measuring the amount of energy reflected and emitted in several discrete portions of the electromagnetic spectrum increases spectral resolution. Satellite scanners are designed either as a passive system or as an active system. Active sensors supply their own source of energy to illuminate features of interest, in contrast to "passive" systems that sense naturally available energy (Lillesand & Kiefer, 1994).

A passive system for remote sensing of ocean colour makes use of a sensor with a narrow field of view, capable of monitoring the radiometric flux reaching the sensor at several selected wavelengths in the visible and near-infrared domains of the electromagnetic spectrum. The sensor, mounted on a satellite, an aircraft or some other remote platform, is aimed at a point on the surface of the earth. Scanning devices on the sensor, and the movement of the platform itself combine to acquire data from different points on the earth. The sensors operate during the daylight hours, and the ultimate source of the light reaching the sensor is the sun (IOCCG No. 3, 2000).

With respect to this basic information, Table-1.1 and Table 1.2 summarizes the characteristics of different sensors (Cracknell, 1999). The remote sensing in coastal and oceanographic studies have been mostly based on the processing and interpretation of these sensors.

Remote sensing of ocean color is based on the measurement of water-leaving radiance in visible part of the electromagnetic spectrum. The total signal detected by the satellite sensor is corrected for the atmospheric noise and then used in empirical algorithms to retrieve the concentrations of phytoplankton pigments in the surface layers of the ocean. Coastal waters are optically complex due to the presence of other constituents like suspended solids and yellow substances, so that interpretation of an optical signal can be rather difficult. To date, remote sensing of ocean colour has focused largely on the relatively simple Case 1 waters, and the algorithms in use generally fail in Case 2 waters.

Coastal Zone Color Scanner (CZCS) being the first ocean-colour sensor, which is used to determine the oceanic chlorophyll is limited by turbidity. LANDSAT and SPOT, on the other hand, lack the overpass frequency to examine the coastal/estuarine dynamics. The new generation of ocean-colour sensors has been designed with improved capabilities (with respect to both spectral and radiometric resolution) like SeaWIFS and MODIS.

The NOAA's Advanced Very High Resolution Radiometer (AVHRR) was designed for meteorological purposes, not for use as an ocean color sensor. The most successful use of AVHRR data in oceanography is the determination of sea surface temperature maps. Although it does not have the sensitivity in the red and near-infrared to examine case-1 water (open ocean), its sensitivity is suitable to examine the patterns in water clarity at turbid estuaries (Stumpf, 1987, 1992, Stumpf & Frayer 1997, Stumpf & Pennock 1989, 1991, Stumpf & Tyler, 1988, Tyler & Stumpf, 1989, Stumpf *et al*, 1999, Woodruff *et al.*, 1999).

Eutrophication due to the supply of organic matter is one of the most important environmental problems of Izmir Bay. Monitoring the levels of chlorophyll - as an indicator for eutrophication – through remote sensing has substantial benefits for the management of eutrophication.

The objective of this study is to construct a model, which estimates the distribution of aquatic chlorophyll-a concentrations in the surface layers of the Izmir Bay with interpretations of remote sensing observations and calculation of primary production based on empirical algorithms. The dataset covers *in situ* measurements carried out in Izmir Bay for the period of 1996-1998 and corresponding AVHRR (NOAA-14) images. Stumpf's (1992) algorithm is used to remove atmospheric effects from the images and retrieve the water leaving reflectances. Then a model is constructed to calibrate those reflectances with the *in situ* chlorophyll-a and attenuation coefficient data. Finally an empirical model is applied to estimate primary production from the remotely retrieved chlorophyll-a data.

Table 1.1 Comparison of Different Sensors

System	SPOT HRV wavelength (µm)		Landsat TM	Landsat MSS	NOAA AVHRR	Nimbus-7 CZCS	Meteosat	SeaWifs
Channel	MS	PAN	wavelength (µm)	wavelength (µm)	wavelength (µm)	wavelength (µm)	wavelength (µm)	wavelength (µm)
1	0.50-0.59	0.51-0.73	0.45-0.52	0.5-0.6 (4)*	0.55-0.680	0.433-0.453	0.4-1.1	0.402-0.422
2	0.61-0.68	X	0.52-0.60	0.6-0.7 (5)	0.725-1.1	0.510-0.530	10.5-12.5	0.433-0.453
3	0.79-0.89	X	0.63-0.69	0.7-0.8 (6)	3.55-3.93	0.540-0.560	5.7-7.1	0.480-0.500
4	X	X	0.76-0.90	0.8-1.1 (7)	10.3-11.3	0.660-0.680	X	0.500-0.520
5	X	X	1.55-1.75	X	11.5-12.5	0.700-0.800	X	0.545-0.565
6	X	X	2.10-2.35	X	X	10.5-12.5	X	0.660-0.680
7	X	X	10.4-12.5	X	X	X	X	0.745-0.785
8	X	X	X	X	X	X	X	0.845-0.885
Resolution	20 m	10 m	chs 1-6: 30 m ch7: 120 m	80 m	1.1 km	825 m	ch 1: 2.4 km chs2,3: 5 km	1.1 km
Revisit	26 days	26 days	16 days	16 days	a few hours	a day or so	half hour	1 day

Table 1.2 Characteristics of New Generation Ocean-Colour Sensors

Sensor	OCM	MODIS-AM	MISR	OCI	OSMI	MERIS	GLI	POLDER-2	MODIS-PM
Platform	IRS- P4	EOS- AM1	EOS- AM1	ROCSAT	KOMPSAT	Envisat	ADEOS- 2	ADEOS- 2	EOS- PM1
Agency	ISRO	NASA	NASA	Taiwan	KARI	ESA	NASDA	CNES	NASA
Country	India	USA	USA	Taiwan	Korea	Europe	Japan	France	USA
Operation Start	Nov. 1998	1999	1999	Feb. 1999	Jul. 1999	Mar. 2000	Jun. 2000	Jun. 2000	Dec. 2000
Operation End	Nov. 2003	Jun. 2003	Jun. 2003	Feb. 2003	Jul. 2002	Feb. 2004	Jun. 2005	Jun. 2005	Dec. 2005
Eq. Crossing Time (h)	12: 00	10: 30	10: 30	09: 00/ 15: 00	10: 50	10: 00	10: 30	10: 30	13: 30
Altitude (km)	720	705	705	600	685	800	803	803	705
Resolution at Nadir (km)	0.36	1	0.25	0.8	0.85	1.2/ 0.3	1/ 0.25	6 x 7	1
Swath (km)	1420	2330	360	704	800	1150	1600	2400	2330

1.1 Definitions in Radiometry Relevant to Ocean Color Viewing from Space

1.1.1 Electromagnetic Spectrum

The fundamental unit in electromagnetic (which may be abbreviated "EM") phenomena is the photon (one form of quanta, from quantum physics). This subatomic particle comprises radiation emitted by matter when it is excited thermally, or by nuclear processes (fusion, fission), or by bombardment with other radiation. Photons, which are massless, move at the speed of light: 300,000 km/sec (186,000 miles/sec). These particles also move as waves and hence, have a "dual" nature (wavelength and frequency) (http:// www.ncsa.uiuc.edu /Cyberia /Bima /spectrum.html).

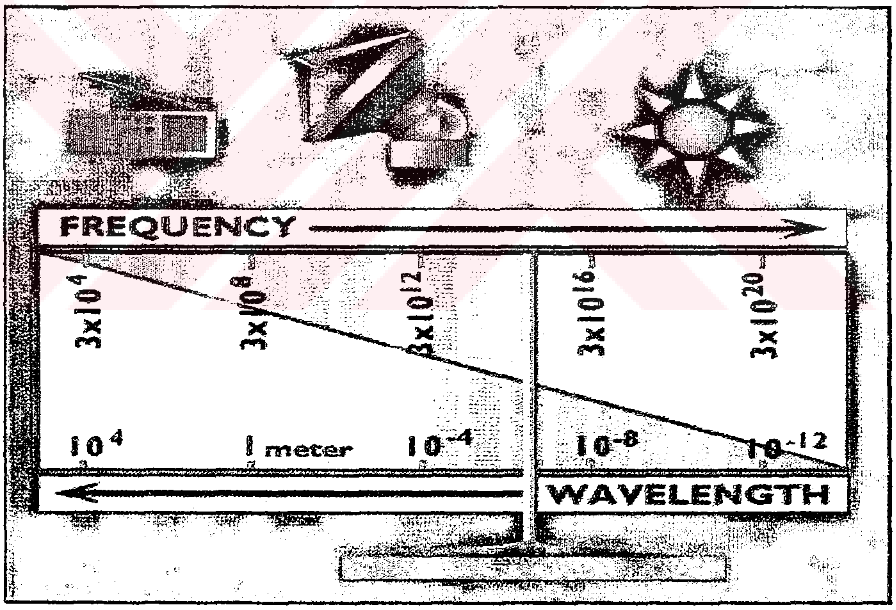

Figure 1.1 Electromagnetic Spectrum (Copied from http://www.ncsa.uiuc.edu/Cyberia/Bima/spectrum.html)

Electromagnetic radiation emitted by the sun encompasses a wide spectral region, which may be divided into several wavelength intervals as follows:

- Gamma rays ($\lambda < 10^{-5}$ μm),
- X-rays (10^{-5} μm $< \lambda < 10^{-2}$ μm),

- Ultraviolet radiation (10^{-2} μm < λ < 0.39 μm),
- Visible radiation (0.39 μm < λ < 0.74 μm),
- Infrared radiation (0.74 μm < λ < 3,000 μm),
- Microwave radiation (λ > 3,000 μm).

The visible radiation is subdivided into seven color intervals:

- Violet (0.39 μm < λ < 0.455 μm),
- Dark blue (0.455 μm < λ < 0.488 μm),
- Light blue (0.488 μm < λ < 0.505 μm),
- Green (0.505 μm < λ < 0.575 μm),
- Yellow (0.575 μm < λ < 0.585 μm),
- Orange (0.585 μm < λ < 0.620 μm),
- Red (0.620 μm < λ < 0.740 μm),

The near-ultraviolet radiation lies in the spectral region (0.28 μm < λ < 0.39 μm); the near-infrared radiation in the spectral region (0.74 μm < λ < 2.4 μm). Together, the near-ultraviolet, visible, and near-infrared spectral intervals form the so-called *optical range* (Bukata *et al.*, 1995).

Satellite sensors on board measure and usually quantify the energy received. A measurement unit system is therefore required and this shall be defined here.

1.1.2 Defining a Direction in Space

The direction of a line through any point on the Earth's surface is defined by two angles (GDTA-B1, 1992):

- the zenith angle θ, between the zenith (point on the celestial sphere located on the observer's ascending vertical) and the direction observed,

- the azimuth angle φ between the North (on the local meridian) and the projection of the line on the Earth's surface.

θ varies along the vertical plane from 0 to $\pi/2$ (0° to 90°), φ varies along the horizontal plane from 0 to 2π (0° to 360°).

1.1.3 Solid Angle

A solid angle $d\Omega$ delimits a cone in space (GDTA-B1, 1992):

$$d\Omega = dS / r^2 \text{ (in steradians, Sr)} \quad (1.1)$$

where dS is the area cut by the cone over a sphere of radius r the center of which is at the apex of the cone (figure 1.2).

The solid angle corresponding to all the space around a point equals 4π Sr.

The solid angle of a revolving cone for which the plane half-angle at the apex is α equals:

$$\Omega = 2\pi (1 - \cos\alpha) \text{ Sr} \quad (1.2)$$

For an observer on Earth, the half-space formed by the celestial arch (in other words an hemisphere) therefore corresponds to 2π Sr ($\alpha=90^\circ$),

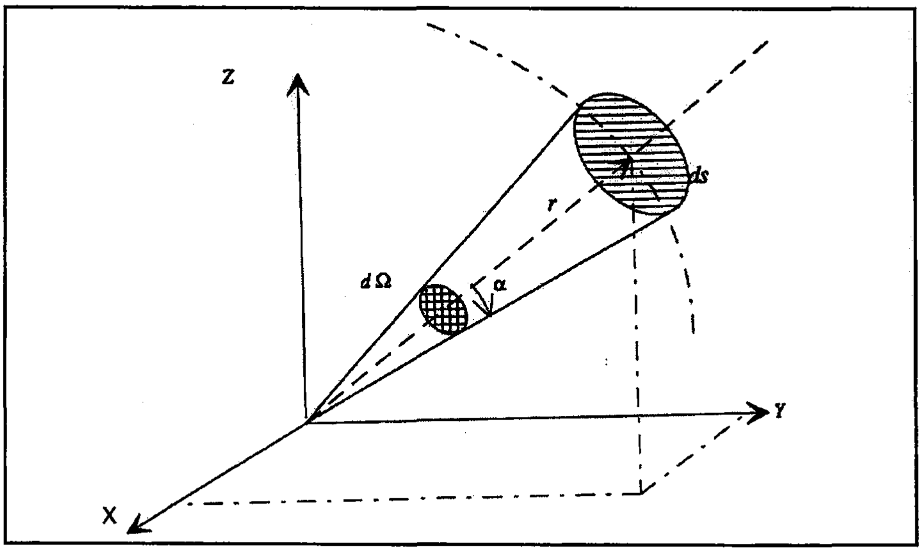

Figure 1.2 Solid angle notion (GDTA-B1, 1992)

1.1.4 Basic Radiometric Quantities

1.1.4.1 Irradiance

The power in an optical beam per unit area (fig.1.3) is termed the radiant flux dϕ. **Irradiance E,** is the power received per surface unit from all directions of a half space (hemisphere) (Lynch, 2000).

$$E = d\phi / dS \text{ (in W.m}^{-2}\text{)} \quad (1.3)$$

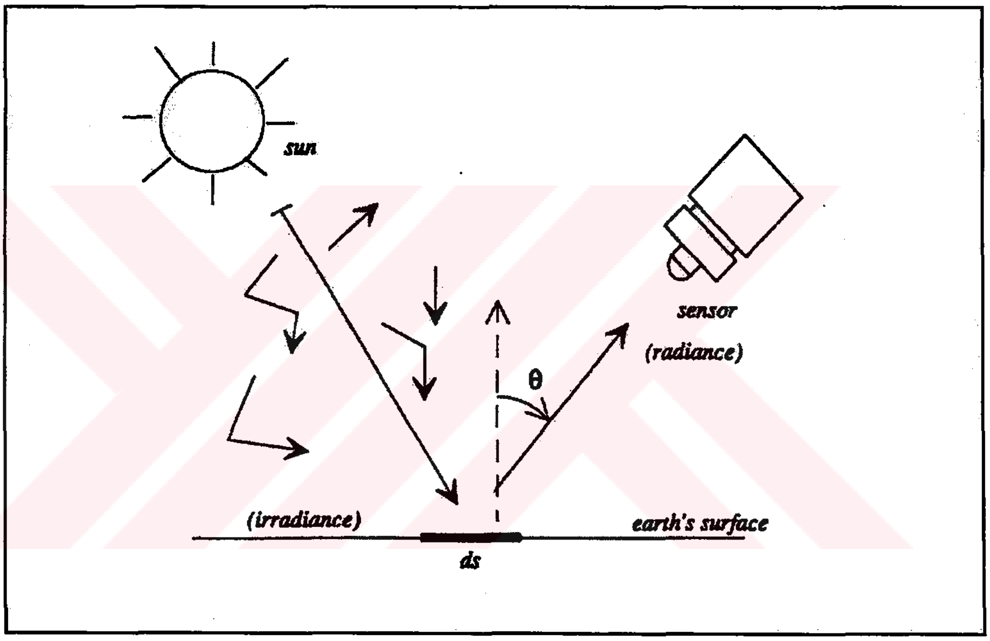

Figure 1.3 Irradiance received by a surface (GDTA-B1, 1992)

1.1.4.2 Radiance

Radiance (L) is the power emitted (dϕ) per unit of the solid angle (dΩ) and per unit of the projected surface (dS cosθ) of an extended widespread source in a given direction (θ) (GDTA-B1, 1992).

$$L = d\phi / (d\Omega.dS.\cos\theta) \text{ (in W.Sr}^{-1}\text{.m}^{-2}\text{)} \quad (1.4)$$

If radiance is not dependent on θ and φ, i.e. if is the same in all directions, the source is said to be Lambertian.

This notion is very important as the energy measured by the sensor is proportional to the radiance of the observed source (Earth's surface).

The element of the Earth's surface dS receives an irradiance E from the upper half space and acts for the sensor as a source of radiance L along a direction θ.

1.1.4.3 Notion of Reflectance

Reflectance is a measurement of a surface's capacity to reflect incident energy.

In remote sensing, specular reflection of sunlight is infrequently observed; it requires a smooth reflecting surface generally larger than the pixel size, such as a free water surface, so that enough energy reaches the sensor for detection (GDTA-B1, 1992).

Energy reflected by the Earth's surface is dependent on:

- The direction of sun with respect to the object observed. This is the direction of incident energy characterized by the angles θ_i, φ_i (the notation θ_o, φ_o is also used);

- The direction along which the sensor views the observed object. This is the direction of incident energy, characterized by the angles θ_r, φ_r. As this is the satellite's viewing direction, the notation θ_v, φ_v is also used.

As reflectance is dependent on both directions, those of the sun and of the sensor, the term bi-directional reflectance is used. This is, moreover, dependent on the observation wavelength λ.

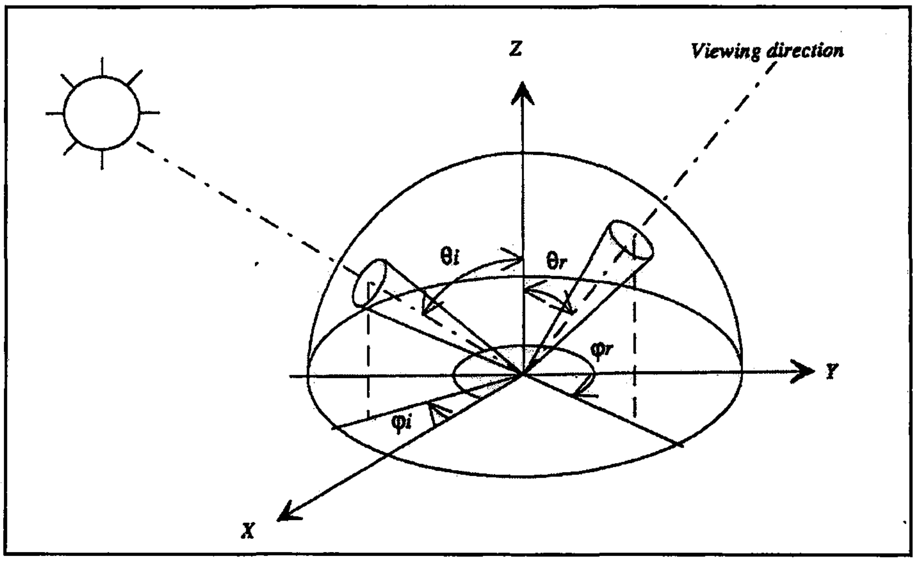

Figure 1.4 The concept of bi-directional reflectance (GDTA-B1, 1992)

Reflectance (R) is defined as

$$R(\lambda) = E_u(\lambda) / E_d(\lambda) \quad (1.5)$$

Where λ is the spectral band or wavelength. E_u is the upwelling irradiance, and E_d is the downwelling irradiance.

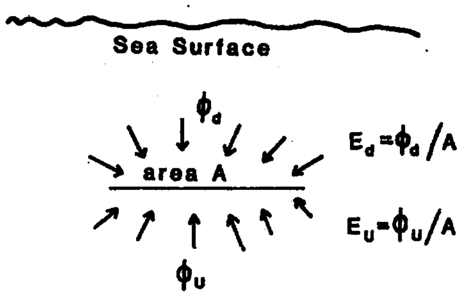

Figure 1.5 Definition sketch: downwelling and upwelling irradiance, E_d and E_u (Robinson, 1997)

A satellite actually detects radiance, namely that portion of the irradiance that is directed toward the sensor.

1.2 Atmospheric Correction

The details of marine optics and optical remote sensing can be found in texts such as Jerlov (1976) and Bukata *et al.* (1995). For remote sensing, the upwelling irradiance, E_u, is equated to the upwelling radiance from the water, L_w, measured by the sensor through

$$E_u(\lambda) = \pi L_w(\lambda) \qquad (1.6)$$

The satellite detects the combined radiance of the water column, the water surface, and the atmosphere (Figure 1.6) . The detected radiance can be expressed as

$$L_*(\lambda) = T(\lambda) L_w(\lambda) + T(\lambda) L_g(\lambda) + L_A(\lambda) \qquad (1.7)$$

where L_* is the radiance detected by the satellite, L_w is the radiance leaving the water column, L_g is the radiance reflected from the water surface (i. e., sunglint), L_A is the radiance from the atmosphere, referred to as path radiance, and T is the atmospheric transmission coefficient.

In (1.7) we are interested in L_w in order to determine the water reflectance. Therefore in order to reliably and consistently determine the characteristics of the water column and the materials within it, we must obtain L_w by correcting for sunglint, L_g, atmospheric effects L_A and T, and the solar zenith angle θ_o.

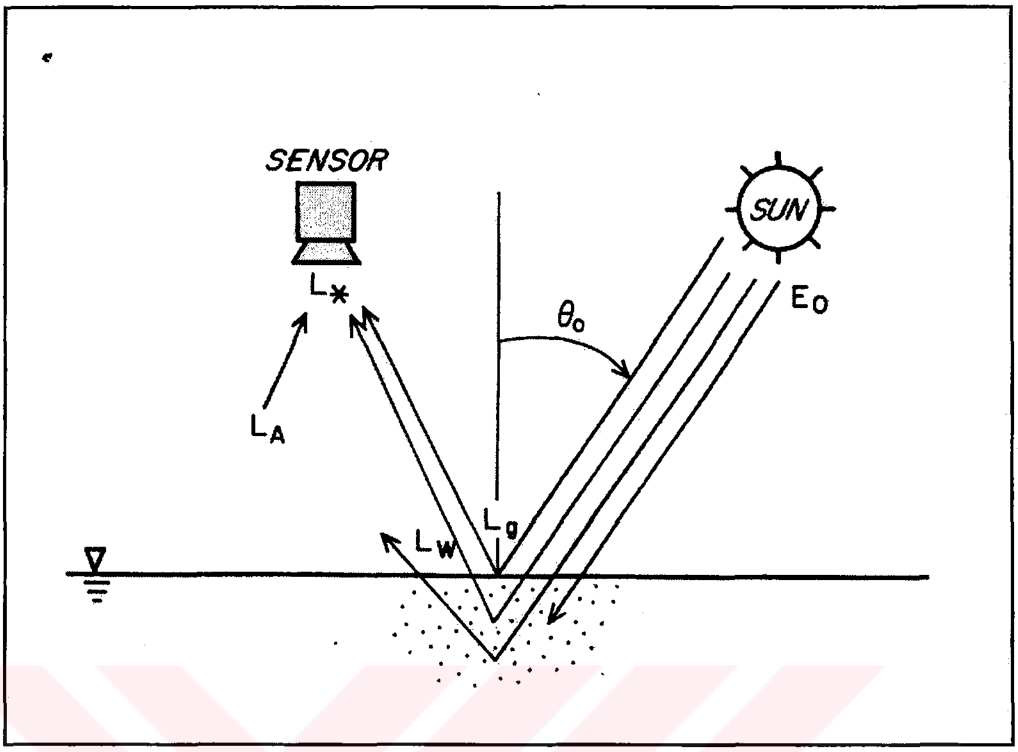

Figure 1.6 Sources of radiance observed at the satellite

1.2.1 Sunglint, L_g

Surface reflection is the specular reflection directly off the water's surface. The skylight reflected back to the sensor is negligible, generally less than 0.2% of the sunlight (Stumpf, 1987). However, reflected sunlight, or sunglint, can be substantial, up to 6% of the incident sunlight.

The intensity of sunglint varies with the surface wave field, therefore it depends on surface winds, currents, and bathymetry. As a result, it will vary considerably throughout a scene, and cannot be adequately approximated. Therefore, the simplest solution to the sunglint problem is to avoid regions containing sunglint. With a wide angle scanner, such as the AVHRR, the image half opposite the sun will always be free of sunglint. For afternoon passes, the eastern half to two-thirds will not contain any sunglint, for morning passes the western portion will be free. In mid-latitudes during the fall and winter, the afternoon passes generally produce images completely free of sunglint owing to the low solar altitude (Stumpf, 1987). For certain applications, the sunglint can be removed. The details of this technique can be found in literature.

1.2.2 Atmospheric Path Radiance, L_A

All radiation detected by remote sensors passes through some distance, or path length, of atmosphere. The net effect of the atmosphere varies with the differences in path length, magnitude of the energy signal being sensed, the atmospheric conditions present and the wavelengths involved. Atmospheric effects are caused principally through the mechanisms of atmospheric scattering and absorption.

Atmospheric scattering is unpredictable diffusion of radiation by particles in the atmosphere. Rayleigh Scattering is common when radiation interacts with atmospheric molecules and other tiny particles that are much smaller in diameter then the wavelength of the interacting radiation. There is a much stronger tendency for short wavelengths to be scattered by this scattering mechanism than long wavelengths. Rayleigh Scattering is the primary causes of haze in imagery. Mie Scattering exists when atmospheric particle diameters essentially equal the energy wavelengths being sensed. Water vapor and dust are major causes of Mie Scattering. Rayleigh scattering dominates under most of the atmospheric conditions (Lillesand & Kiefer, 1994).

Gasses are responsible for the selective absorption of some wavelengths;

- Ultraviolet and any radiation less than 0.3μm is absorbed by Ozone.
- Visible and NIR radiation is only absorbed to a small extent by gasses.

The path radiance can be expressed as

$$L_A = L_r + L_a \tag{1.8}$$

Where L_r is the Rayleigh path radiance and L_a is the aerosol path radiance. Elimination of path radiance will be discussed in the next section.

1.2.3 Atmospheric Attenuation, T

T is that proportion of the surface-leaving radiance, which is not scattered out of the field of view, and known as the direct or beam transmittance of the atmosphere. T also depends on the scattering and absorption properties of the atmosphere.

1.3 Marine Optics

In general marine waters can be classified into two main categories (known as case 1 and case 2 waters) according to the kind of constituents that shape their optical properties. The first is usually found in the pelagic zone and is optically dominated by biological agents such as planktonic pigments. The second category often occurs in coastal zones with high coastal runoff, where biological agents are accompanied by suspended sediments, degrading terrigenous organic materials and other particulate or dissolved substances.

The spectral signature of the water-leaving radiance can be assessed directly by ocean-color remote sensing (once atmospheric influences are corrected for). This signature, which describes the color of water, is determined by the inherent optical properties of the constituents i.e. spectral absorption and scattering properties. The concentrations of the constituents can only be assessed indirectly by remote sensing, through the influence of their inherent optical properties on the spectral signature of the light remitted from the water body. The concentration of a constituent of the water body can be calculated either from empirical regressions, or from bio-optical models, which are implemented using experimental data on the spectral variations of specific optical properties. For case 2 waters, the difficulty is that the relationship between ocean color and the constituents of the water may vary regionally or seasonally, according to the composition of algal species, size distribution of phytoplankton cells, mineral composition of the inorganic particles in suspension or the chemical composition of dissolved organic substances. Therefore, Case 2 algorithms are typically local or regional in nature. Primary production can also derived from satellite data (IOCCG No. 3, 2000).

Underwater light availability is one of the major parameters that is important for aquatic primary production. Light penetrating into the water is reduced exponentially by absorption and scattering (The Open University, 1997):

Absorption involves the conversion of electromagnetic energy into other forms, usually heat or chemical energy (e.g. photosynthesis). The absorbers in seawater are:

- Algae (phytoplankton) using light as the energy source for photosynthesis.
- Inorganic and organic particulate matter in suspension (other than algae).
- Dissolved organic compounds
- Water itself.

When phytoplankton cells decompose in the water column (or in the bottom sediments), the organic matter is chemically transformed, through microbial action on time scales of days to weeks, to CO_2 and inorganic nitrogen, sulfur and phosphorus compounds. Over 80% of the principal remains of the decomposed phytoplankton cells (under aerobic conditions) result in such substances as CO_2, CH_4, NH_3, and H_2O, among others. In addition, the decomposition process results in the creation of a variety of complex polymers generally referred to as the so called water humus, or humic substances. These humic substances comprise both water soluble and water-insoluble fractions, the insoluble fraction, referred to as humin being present as suspended particulates of a variety of particle sizes and molecular weights. The water-soluble fraction comprises dissolved organic carbon in the forms of humic acid and fulvic acid. The soluble and insoluble fractions of humic substances are quite similar in chemical composition, albeit different in molecular weight. The presence of water-soluble humic substances in natural waters is readily apparent in inland and coastal waters (when their presence is not otherwise obfuscated by suspended particulates) by varying degrees of yellowness that are observable in such waters. This yellowness is a consequence of the temperature dependent Maillard reaction involving amino acids, carbonates, and phenol-bearing matter. In the presence of an alkaline medium the Maillard reaction leads to the formation of yellow and brown melanoids. These melanoids, however, comprise only a small fraction ~ (10-40)% of the aquatic Dissolved Organic Matter. As a consequence of this yellow hue, the dissolved aquatic humus is generally referred to as yellow substance (YS), although such humic matter has been historically referred to in the literature by a variety of terms such as gelbstoff, aquatic humic matter, yellow organic acids, humolinnic acid, gilvin, and others (Bukata *et al.*, 1995).

Scattering simply changes the direction of electromagnetic energy, as a result of multiple reflections from suspended particles. Obviously, the greater the amount of suspended matter (i. e. the more turbid the water) the greater degree of absorption and scattering.

The basic principle of the beam transmittance is to produce a parallel beam of light which, after passing a water path of fixed length, impinges on a detector. The beam transmittance meter is designed for the purpose of measuring attenuation coefficient, c (m^{-1}), defined as absorption coefficient plus total scattering coefficient (Jerlov, 1976).

$$c = c_w + b_p + a_p + a_y \qquad (1.9)$$

where c_w is the attenuation by the water itself, b_p, is the scattering due to particles, a_p absorption due to particles and a_y is the absorption due to yellow substances in water.

The reflectance from the water column, an apparent optical property, is described in terms of its inherent optical properties, absorption (a) and backscatter (b_b) by Gordon *et al.* (1975) (Woodruff *et al.*, 1999). For an optically-deep (<10% of surface radiance reaching the bottom), vertically homogenous water column, reflectance is expressed as:

$$R_w(\lambda) \equiv \frac{E_u}{E_d} = \frac{b_b}{b_b + a} \qquad (1.10)$$

The greater the backscattering (b_b) the greater the reflectance, while increased absorption (a) decreases the reflectance. We note, however, that a very low absorption does not in itself lead to a high reflectance, since there must be scatterers present. Thus both clear water and turbid water containing strongly absorbent material have low reflectances (Robinson, 1997).

Chlorophyll-a concentration is often high in Case 2 waters, ranging from less than 1 to 100 mg m^{-3} or higher. At these high chlorophyll levels, there would be a strong fluorescence signal from chlorophyll-a centered at around 685 nm. Fluorescence per unit chlorophyll varies greatly, and thus there is some uncertainty about the interpretation of this signal. However, it does provide an indication of the abundance and productivity of phytoplankton (IOCCG No. 3, 2000).

Coastal waters tend to be particularly turbid. The suspended load brought in by rivers is kept in suspension by waves and tidal currents, which also stir up sediment already deposited on the bottom. In addition, rivers supply coastal waters with nutrients that support phytoplankton growth, and with dissolved organic compounds. By contrast, the water tends to be particularly clear in central oceanic regions, especially where concentrations of nutrients are low and where there is little biological production. The signature of the suspended particles is strongest in the 550 to 600 nm spectral range (IOCCG No. 3, 2000).

The reduction of light in the water column can be expressed in terms of the (vertical) extinction coefficient (K_d, also called attenuation coefficient, m^{-1}):

$$I_d = (I_0)e^{(K_d)d} \qquad (1.11)$$

Where I_0 is the incoming light intensity, I_d is the light intensity at depth d. There are two approaches (one direct and one indirect) to estimate the average extinction coefficient in a given water column. The direct approach involves the actual measurement of light intensity at different depths using a suitable sensor. The indirect estimation can be done from Secchi disc reading S, in meter), using an empirical relation (Parsons *et al.*, 1984):

$$K_d = f / S \quad (1.12)$$

With f ranging from 1.4 in turbid coastal waters, 1.7 in offshore neritic waters, and 2.2 in oligotrophic ocean waters (Gieskes, 1991).

The role of light on photosynthetic rate is illustrated in figure 1.7.

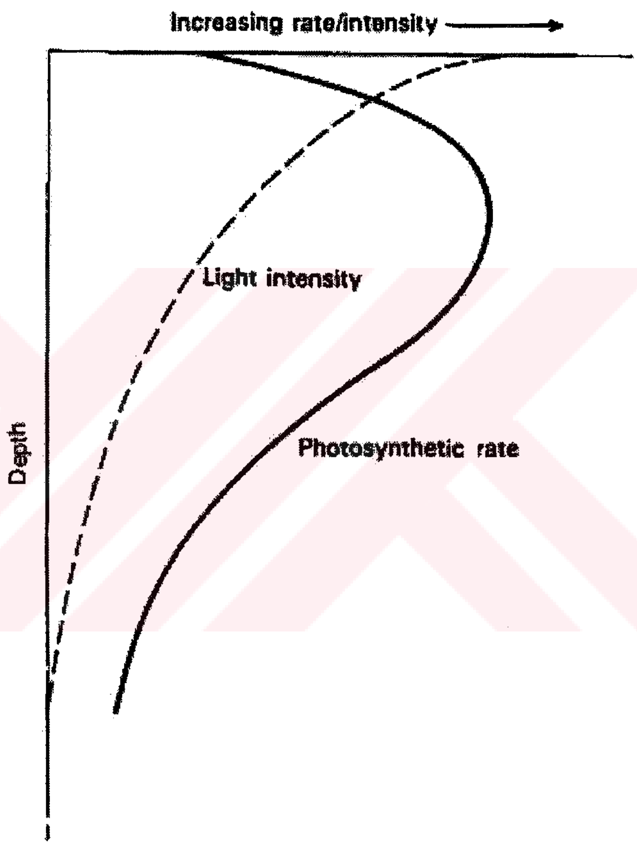

Figure 1.7 Generalized sketch of vertical profiles of light availibility and corresponding rate of photosynthesis in water columns in which phytoplankton are uniformly distributed in the vertcal dimension.

1.4 Estimating Primary Production

Phytoplankton constitutes the beginning of the food chain for most of the living organisms on the planet. Phytoplankton as revealed by the ocean color frequently shows scientists where ocean currents provide nutrients for plant growth. In addition, the plant show where pollutants toxify the ocean and prevent plant growth, and where subtle changes in the climate-warmer or colder more saline or less saline water masses affect phytoplankton growth. Since phytoplankton depends upon specific conditions for growth, they frequently become the first indicator of a change in their environment.

The estimation of primary productivity from satellite measurements of ocean color is critical for developing an understanding of how ocean biological processes affect, and are affected by, changes in atmospheric radiative budgets and global biogeochemical cycles (Falkowski *et al.*, 1998).

Photosynthetic processes occur in both oceanic and terrestrial ecosystems. The approximate magnitude of net carbon fixation and biomass in the two environments is known within approximately a 30% error (Table 5.1). It is clear from comparison of the two ecosystems that: a) the absolute magnitude of carbon fixation attributed to marine photosynthetic organisms accounts for approximately 40% of the global total, b) oceanic photosynthetic organisms turn over far more rapidly than their terrestrial counterparts, and c) marine photosynthetic organisms, composed almost entirely of single-celled phytoplankton, account for less than 1% of the total global plant biomass. Thus, oceanic photosynthetic organisms are extremely efficient in fixing carbon compared to terrestrial plants and they mediate a large flux of organic carbon into the ocean interior. This carbon flux sustains a steady-state air-sea gradient in inorganic carbon and is often referred to as the 'biological pump' as stated by Volk & Hoffert (1985) (Falkowski *et al.*, 1998).

Table 1.3 Comparison of Productivity and Biomass in Marine and Terrestrial Ecosystems.

Ecosystem	Total Net Primary Productivity (10^{15} grams/year)	Total Living Plant Biomass (10^{15} grams)	Turnover Time (years)
Marine	25 – 50	1 - 2 0.	0.2 - 0.08
Terrestrial	50 – 75	600 – 800	8 - 16

1.5 Photosynthesis

Photosynthesis is a process resulting in the biological combination of chemical compounds in the presence of light. It commonly refers to the production of organic substances (primarily sugars) from carbon dioxide and the water residing within green plant cells, provided the cells are sufficiently irradiated to allow plant chlorophylls to act as an agent in transforming radiant energy into an organic compound. The natural and cultivated flora of a region provides the principal photosynthetic organisms to the terrestrial biome. The benthic and planktonic algae as well as higher forms of plant life and some species of bacteria provide the principal photosynthetic organisms to the aquatic biome. To capture radiant light and use the light energy to form organic chemical compounds, these photosynthetic organisms contain certain pigments within intricate sub cellular plant structures known as chloroplasts or intricate bacterial substructures known as chromatophores (Bukata *et al.*, 1995). Photosynthesis can be represented as follows:

$$\xrightarrow{} \text{photosynthesis}$$

$$6CO_2 + 6H_2O + \text{energy} \Leftrightarrow C_6H_{12}O_6 + 6O_2 \text{ (gas)}$$

$$\leftarrow \text{respiration}$$

1.6 Phytoplankton Photosynthesis (Primary Production)

Primary production is the chemical energy contained within an ecosystem, as direct result of photosynthesis. Primary productivity is the sum of all photosynthetic rates within that ecosystem. For the assessment of aquatic primary production, therefore, the single most important parameter is the daily integral of photosynthesis occurring within the entire water column. Historically, this photosynthesis has been determined by *in situ* determinations of oxygen production or carbon (^{14}C) uptake at a variety of depths. Primary production is generally recorded in units of g Carbon $m^{-2}\,yr^{-1}$. Since phytoplankton are the principal photosynthesizers in Case 1 waters, it is not unreasonable to assert that phytoplankton photosynthesis and primary production are interchangeable nomenclature for mid-oceanic systems. Such is not the case, however, for non-Case 1 waters wherein terrestrially derived organics and photosynthesis by macrophytes and periphyton can dominate aquatic carbon budgets (Bukata *et al.*, 1995).

Primary production by phytoplankton forms the basis of marine food webs in oceanic and many coastal waters. Knowledge of rates of primary production is critical for improved understanding and management of pelagic and benthic ecosystems, wild fisheries and aquaculture, and impacts of added nutrients (eutrophication) (IOCCG No. 3, 2000).

The diversity of phytoplankton affects the photosynthetic processes directly due to the optical absorption properties of the cells. Biological diversity is an indirect response to environmental changes. Ocean physics and chemistry change on daily, seasonal, annual, and climatological time scales and affect the depth of mixing (and hence, the light regime), nutrient concentration, and temperature (Falkowski *et al.*, 1998).

Light intensity strongly affects the rate of photosynthesis. The relationships required to estimate aquatic photosynthesis (Smith, Fee, Vollenweider, Patten, Bannister) are:

1. Irradiance as a function of time, i.e., I vs. t

2. Photosynthesis P as a function of irradiance, i.e., P vs. I

3. Irradiance as a function of aquatic depth, I vs. z

Relationship 1 is obtained by direct measurement in air above the water body. Relationship 3 is determined from the attenuation coefficient, K_d, is a function of solar angle θ (i.e., time t). Bukata *et al.*, however, conclude that while the diurnal variation of K_d has a significant impact on calculated daily irradiation (integration at a particular depth of subsurface irradiance over daily hours), its impact on estimates of primary production is quite small. On-site values of K_d (θ) are obtained from depth profiles of the subsurface irradiance. The essence of the primary production (phytoplankton photosynthesis) calculation is relationship 2, namely P as function of irradiance (Bukata *et al.*, 1995).

The photosynthesis/light curve (or P vs. I curve) shown in Fig. 1.8 is a convenient reflection of environmental effects on photosynthesis.

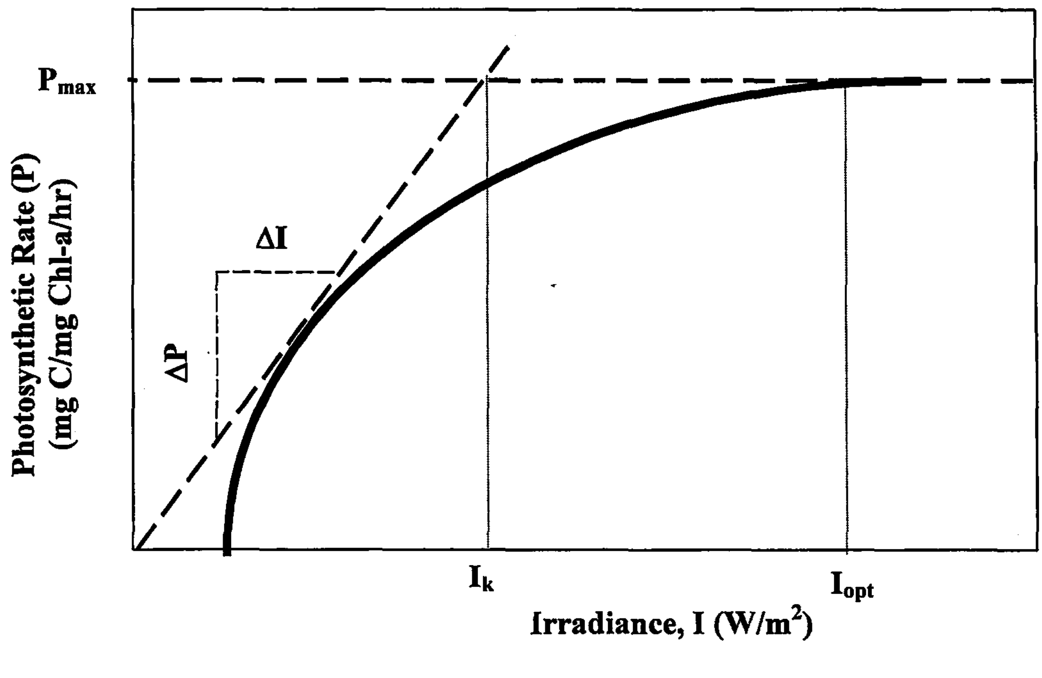

Figure 1.8 Schematic representation of the Photosynthesis/light curve (P vs I curve)

Photosynthesis increases with increasing light intensity up to some asymptotic value, P_{max} where the system becomes light saturated. The two most important properties of the curve are the slope ($\alpha = \Delta P/\Delta I$) and P_{max} , in which the latter is also called the assimilation number (or assimilation index) (Parsons *et al.*, 1984).

Absolute primary production at a certain depth, can be recovered by:

$$P_a(z) = [Chlorophyll(z)] \cdot [P(z)] \quad (1.13)$$

The total daily phytoplankton photosynthesis (approximate primary production) throughout the water column would then be given as the integration of the P versus I curve over the depth of the photic zone and the length of the daylight period (Bukata *et al.*, 1995).

$$PP = \int_{t_d}^{t_s} \int_{z_{0.01}}^{z_{1.0}} P_a(z,t)\,dz\,dt \quad (1.14)$$

where;

$z_{1.0}$ = depth of the 100% irradiance level, i.e., just beneath the air-water interface

$z_{0.01}$ = depth of the 1% irradiance level, below which occurs no significant contribution to primary production

t_d = time of local dawn

t_s = time of local sunset

To a first order approximation, the concentration of phytoplankton pigments can be quantitatively related to the photosynthetic rate. If the quantum yield of photosynthesis was constant, photosynthetic rates would be directly proportional to the rates of irradiance and chlorophyll-a concentrations. Chlorophyll is a pool while primary productivity is a flux. To derive a flux from a pool, a time related variable must be incorporated. Time dependent models of photosynthesis are developed by incorporating irradiance, where the transfer function is the quantum yield. Quantum yields are not constant and a wide range productivity models have been developed to estimate phytoplankton photosynthesis from satellite-derived chlorophyll fields; each differing with respect to assumptions made regarding the variability in quantum yields (Falkowski *et al.*, 1998).

Algorithms used to calculate total primary production from satellite remote sensing data range from simple empirical relationships to complex analytical models. Empirical models make broad generalizations about the relationships between satellite-based estimates of upper ocean chlorophyll and integrated production and generally require additional parameterization, or tuning, when extended to regions, or even seasons within a region, beyond those from which they were derived. Analytical models attempt to calculate photosynthesis using first principles of phytoplankton photophysiology and light penetration through the water column, an approach that adds both physical rigor and increasing complexity. In a sense, analytical and empirical approaches are not disparate as may first appear, since many of the photoadaptive coefficients used in analytical models, such as the initial slope (α) or the maximum rate P_{max}, are simply empirically-derived coefficients based on shipboard measurements. In addition, all productivity models rely on empirical relationships between plankton population seen by a satellite and the photosynthetic populations in the deeper regions of the water column invisible to the satellite. In 1994, the international ocean sciences community established, under the sponsorship of the SeaWiFS program, an open Ocean Primary Productivity Working Group (OPPWG) to help evaluate the variations and similarities between myriad models. The fundamental goal of the OPPWG is to iteratively develop; compare, test, and implement standardize algorithms that calculate oceanic photosynthesis from satellite observations of ocean color. By using standard input variables such as chlorophyll-a, the primary production algorithm selected will not be dependent on a specific sensor. This effort will provide the framework for quantifying ocean biological processes in the 21st century (Falkowski et al., 1998).

1.7 Primary Productivity Models

As a point of reference, the estimation of daily phytoplankton photosynthesis within the euphotic zone per unit of ocean surface is a common application for all primary production models (Behrenfeld & Falkowski, 1997).

Each category in Table 1.4 includes a photoadaptive variable (i.e., Φ, φ, P^b (z), $P^b{}_{opt}$ corresponding to the resolution of the described light field. Φ and φ are chlorophyll-specific quantum yields for absorbed and available photosynthetically active radiation (PAR), respectively. Wavelength-resolved models (WRMs) and wavelength-integrated models (WIMs) are parameterized using measurements which approximate net photosynthesis and therefore, require subtraction of daily phytoplankton respiration (R) to calculate (ΣPP). Time integrated models (TIMs) and depth integrated models (DIMs) are ideally, parameterized using measurements conducted over 24 hr which approximate net primary production and thus, do not require subtraction of respiration. $P^b(z)$ and $P^b{}_{opt}$ are chlorophyll specific photosynthetic rates; the asterisk (*) indicates normalization to chlorophyll concentration. A generic classification of primary production models illustrates that the fundamental difference in model structure is related to the level of integration (Falkowski *et al.*, 1998).

Satellite measurements of ocean color can provide estimates of upper ocean pigment concentration. However, chlorophyll is not uniform throughout the water column in most regions of the world ocean and frequently subsurface chlorophyll maxima are observed near the bottom of the upper mixed layer. A considerable effort has gone into developing empirical algorithms that relate satellite-based estimates of phytoplankton pigment concentration to the vertical structure. Often, this exercise has been concurrently accompanied by optical models that permit the explicit calculation of spectral irradiance at any depth at any time throughout the day. Hence, time dependent, depth resolved, spectral models (i.e. WRMs) were developed to calculate photosynthetic rates at each point in the water column throughout the day. These algorithms are often parameterized with local in situ measurements of photosynthesis in relation to irradiance and inherently emphasize the role of light absorption in controlling photosynthetic rates (Falkowski *et al.*, 1998).

Table 1.4 Classification system for daily primary productivity (ΣPP) models based on implicit levels of integration (Falkowski *et al.*, 1998).

Model Category	Generalized Model Structure
WRMs	$\sum PP = \int_{\lambda=400}^{700} \int_{sunrise}^{sunset} \int_{z=0}^{z_{eu}} \varphi(\lambda,t,z) PAR(\lambda,t,z) a^{*}(\lambda,z) Chl(z) d\lambda dt dz - R$
WIMs	$\sum PP = \int_{sunrise}^{sunset} \int_{z=0}^{z_{eu}} \Phi(t,z) PAR(t,z) Chl(z) dt dz - R$
TIMs	$\sum PP = \int_{z=0}^{z_{eu}} P^{b}(z) PAR(z)(DL) Chl(z) dz$
DIMs	$\sum PP = P_{opt}^{b} PAR(0)(DL) Chl(z_{eu})$

z_{eu} is depth of the euphotic zone
t is time
DL is day length

There are also productivity algorithms based on parameterizations of daily integrated primary productivity. These algorithms can be either depth-resolved or depth integrated. Parameterization of these algorithms is based on measurements, which inherently integrate variable photosynthetic rates over a day and often over depth. Both types of algorithms can be modeled in terms of two or three parameters: an initial light-limited productivity rate, a water column maximum value for productivity normalized to chlorophyll, and possibly a parameter characterizing photoinhibition at high light. The advantage of these semi-integrated algorithms is that their parameterization is more consistent with the level of integration associated with satellite data and in situ measurements. One could therefore argue that characterization of local scale variations in photosynthesis-irradiance parameters is unnecessary, since satellite data are already integrated at the local scale (Falkowski *et al.*, 1998).

1.8 Depth integrated models

A complete list of variables included in DIMs can be derived intuitively with only a fundamental understanding of phytoplankton photosynthesis. Explicitly, any model of water-column photosynthesis is expected to require a measure of depth-integrated phytoplankton biomass, which, for practical purposes, can be estimated using the surface chlorophyll-a concentration (C_{surf}) scaled to the depth of the euphotic zone (Z_{eu}). Also, an irradiance-dependent function F and a photoadaptive yield term ($P^b{}_{opt}$) are required to convert the estimated biomass into a photosynthetic rate. Finally daylength DL is included as a variable, because DIMs are often parameterized and tested using observational data from multiple-hour incubations scaled to daily rates using daylength. The complete form of a DIM would be:

$$\Sigma PP = C_{surf} \times Z_{eu} \times P^b{}_{opt} \times DL \times F \qquad (1.15)$$

Talling (1957) derived a DIM from in situ vertical distributions of Pz and the photosynthesis-irradiance relationship originally presented by Smith (1936) (Behrenfeld & Falkowski, 1997). A second DIM was published in 1957 by Ryther and Yentsch.

The broken line in figure 1.9 shows the relative photosynthesis, R beneath a square meter of sea surface (the right hand ordinate) for different values of total daily radiation incident to the sea surface. For homogenous distributions of chlorophyll concentrations with depth, and assuming that 3.7 g Carbon are assimilated per hour at light saturation for each gram of chlorophyll, the phytoplankton production in $gCm^{-2}day^{-1}$ is calculated from:

$$P = \frac{R}{K_d} \times C \times 3.7 \qquad (1.16)$$

where C is g chlorophyll per m^3, K_d is extinction coefficient, per meter.

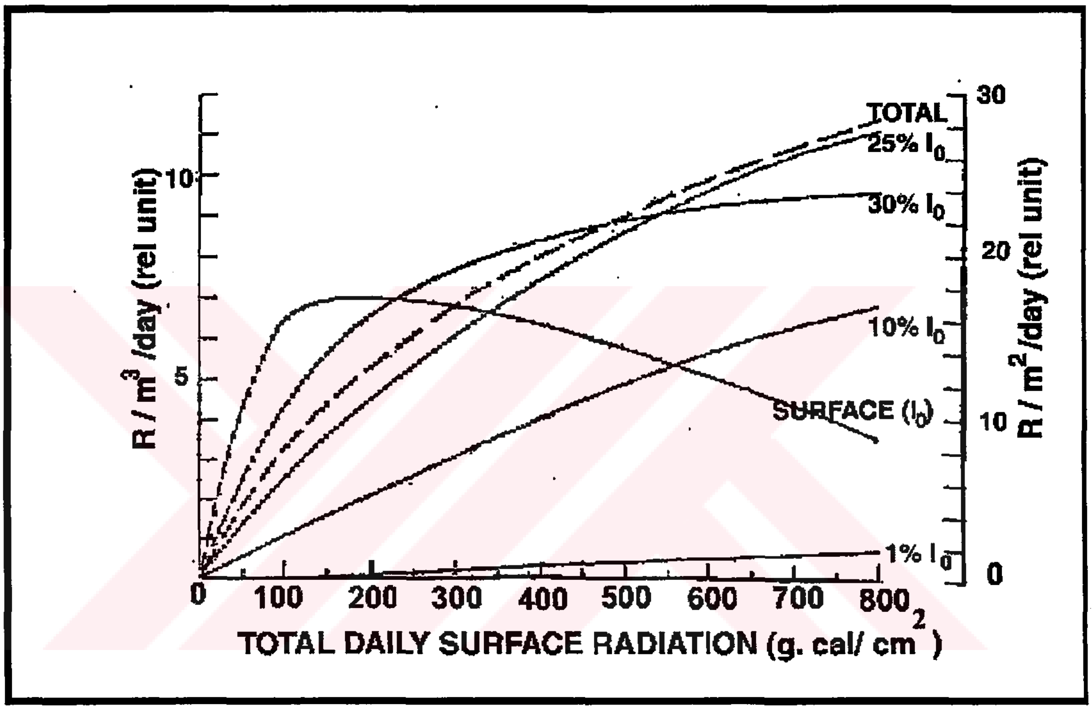

Figure 1.9 **The relation between total daily surface radiation and daily relative photosynthesis (R) beneath a unit of sea surface (broken line) and at the depths where the surface light intensity is reduced by specified amounts (solid lines) from Ryther & Yentsch (1957).**

If the phytoplankton are not distributed evenly with depth, photosynthesis must be calculated separately for several depths. The solid lines in figure 1.9 show daily photosynthesis per m^3 (left hand ordinate, R_d) relative to photosynthesis per m^3 per hour at light saturation at the sea surface, I_0, and at the depths where the surface light intensity is reduced to 50%, 25%, 10%, and 1% respectively. An absolute value for daily photosynthesis ($gCm^{-3}day^{-1}$) at each of these depths may be obtained from the expression:

$$P_d = R_d \times C_d \times 3.7 \qquad (1.17)$$

where C_d is g chlorophyll per m^3 at depth, d.

As an initial estimate, Ryther and Yentsch (1957) assigned P^b_{opt} a constant value of 3.7 mgC $(mgChl)^{-1}$ h^{-1}, which Cullen (1990) suggested should be revised to 4.8 mgC $(mgChl)^{-1}$ h^{-1} due to improvements in the determination of pigment concentrations (Behrenfeld & Falkowski, 1997).

In 1959, Wright developed another DIM and found that the average value of F was ~0.54, with a range of 0.35-0.63. In accordance with the studies of Rhode *et al.* (1958) and Rhode (1966) F was in a range of 0.46-0.65 and using a value of 0.5 for F would not introduce significant errors to the estimates of ΣPP. Vollenwieder (1966) published the standard DIM equation from expressions for the depth dependent changes in net photosynthesis. His basic formulation for ΣPP was (Behrenfeld & Falkowski, 1997):

$$\sum P = F(i) \times \frac{P_{opt}}{\in} \qquad (1.18)$$

as written in his original nomenclature. When transferred to the variables defined in this thesis $\Sigma P \equiv \Sigma PP$, $P_{opt} \equiv P^b_{opt} \times C_{surf} \times DL$, $\in \equiv k_d$, and $F(i) \equiv 4.6 \times F$.

Vollenwieder (1970) separated the compound variable, k_d, into attenuation due to phytoplankton chlorophyll (η_π) and that due to water, dissolved organics, and detritus ($\in$) (Behrenfeld & Falkowski, 1997).

$$\sum A = \frac{\pi_{opt} \times b}{\in + \eta_\pi \times b} \times F\left(\frac{I_0}{I_k}\right) \qquad (1.19)$$

where $\Sigma A \equiv \Sigma PP$, $\pi_{opt} \equiv P^b_{opt} \times DL$, $b \equiv C_{surf}$, and $F(I_0/I_k) \equiv 4.6 \times F$.

Megard (1972) proposed the following DIM (Behrenfeld & Falkowski, 1997):

$$\Sigma P = a \times \exp(-k_n n) \times p_{max} \qquad (1.20)$$

where $\Sigma P \equiv \Sigma PP$, $a \equiv 4.6 \times F \times \in^{-1}$, $k_n n \equiv \eta_\pi \times b$, $p_{max} \equiv P^b{}_{opt} \times C_{surf} \times DL$ and he calculated an average k_n value of 0.013.

Bannister (1974) equated ΣPP to the realized fraction of light absorbed by phytoplankton and a maximum obtainable limit to daily production when all available radiation is absorbed by phytoplankton (Behrenfeld & Falkowski, 1997):

$$\Pi = \Psi \times \frac{k_c C}{k_c C + k_w}, \tag{1.21}$$

where $\Pi \equiv \Sigma PP$, k_c and $k_W \equiv \eta_\pi$ and $\in$ respectively and C is the chlorophyll concentration. The upper limit to production (Ψ) was estimated as

$$\Psi = 2.3 \times P_{max} \times k_c^{-1} \tag{1.22}$$

where $P_{max} \equiv P^b{}_{opt} \times DL$

Eppley *et al.* (1985) used standard ^{14}C-based estimates of daily productivity (Π, in units of $mgCm^{-2}d^{-1}$), along with average chlorophyll-a concentrations (C_K, in units of $mgChl\ m^{-3}$), collected from a range of marine environments during various seasons, to calculate, using linear regression analysis, the empirical relationship (Falkowski *et al.*, 1998):

$$Log_{10}(\Pi)=3.0 + 0.5 log_{10}(C_K), \tag{1.23}$$

Which was revised using the data of Berger (1989) to:

$$Log_{10}(\Pi) = 2.793 + 0.559 log_{10}(C_K) \tag{1.24}$$

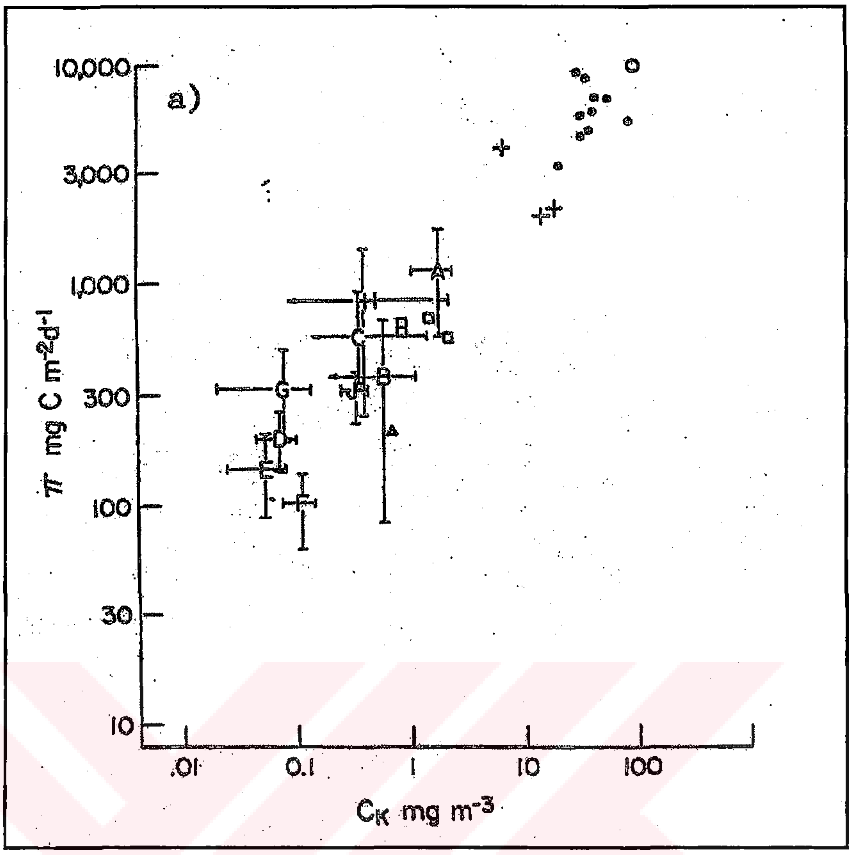

Figure 1.10 Empirical relationship between surface chlorophyll concentration (C_K) and depth integrated primary production (Π) from Eppley *et al.* (1985).

A wide range of marine environments were represented in the data sets compiled by Berger (1989) and Eppley *et al.* (1985). Simply expanding the number of represented environments would likely not reduce variability in parameterization values of these seasonal productivity algorithms. Two approaches have been taken to expand the seasonal and spatial range of a given productivity algorithm (Falkowski *et al.*, 1998):

1. Increase the integration time for primary production (decreased complexity); and

2. Increase the number of algorithm parameters (increased complexity) to reflect the primary factors resulting in the observed variability.

In 1990, Banse & Young applied the DIM of Rodhe (1966) to describe variability in ΣPP observed in the eastern tropical Pacific Ocean as (Behrenfeld & Falkowski, 1997):

$$P_t = 2.3 \times (P/Chl)_{opt} \times Pig_{sat} \times k^{-1} \quad (1.25)$$

where $P_t \equiv \Sigma PP$, $Pig_{sat} \equiv C_{surf}$ and $k \equiv k_d$. They used the variable $(P/Chl)_{opt}$ as a correlate for $P^b{}_{opt}$.

Platt & Sathyendranath (1993) used dimensional analysis to derive the relationship (Behrenfeld & Falkowski, 1997):

$$P_{z,t} = \frac{B \times P^b_m \times D}{K} \times f(I^m_*) \quad (1.26)$$

where $P_{z,t} \equiv \Sigma PP$, $B \equiv C_{surf}$ for a uniformly distributed biomass, $D \equiv DL$, $K \equiv k_d$, $P^b{}_m \equiv P^b{}_{max}$ and $I^m{}_*$ = the ratio of modeled clear sky irradiance at local noon to E_k.

In DIMs differences in F functions are due to variations in the photosynthesis-irradiance-type equation used to describe P or assumptions regarding the importance of an irradiance-dependent term in modelling ΣPP. For most practical purposes, changes in surface PAR have a relatively minor effect on variability in ΣPP. Thus, increasing the time, depth, or wavelength resolution in model descriptions of PAR will not significantly improve estimates of ΣPP, unless the increased resolution directly improves the characterization of the photoadaptive variables $E^*{}_k$ or $P^b{}_{opt}$. Reported differences in DIM performance do not result from fundamental differences in model structure, but rather reflect differences in the parameterization of the photoadaptive variable (Behrenfeld & Falkowski, 1997).

DIMs implicitly assume a vertically homogenous distribution of biomass, which has long been recognized as an oversimplification. Sensitivity analyses by Platt *et al.* (1991) and Antoine *et al.* (1996) indicated that model estimates of ΣPP differed by

<20% for calculations based on structured C, profiles compared to vertically homogenous distributions (Behrenfeld & Falkowski, 1997).

Analytical models incorporate a larger degree of biological and physical detail, placing them at the other end of the parameterized algorithm spectrum. Concepts and mathematical formulations of analytical models are relatively simple, but uncertainties and excessive degrees of freedom in the actual parameterization allow for a number of diverse approaches in model development. The general approach of analytical models can be illustrated using two relatively well known bio-optical models, speciafically the Bedford (Platt *et al.* 1991) and LPCM (Morel 1991) models The basic procedure for both the Bedford and LPCM models is to use information on sea surface chlorophyll concentration to (Falkowski *et al.*, 1998):

1. Fist, estimate the vertical distribution of chlorophyll;

2. Second, use these modeled chlorophyll profiles and either measurements of surface irradiance or modeled irradiance based on location and date to calculate, from physical principles of light attenuation, the vertical distribution of spectral irradiance; and then

3. Third, calculate depth-dependent primary production using the modeled chlorophyll normalized photosynthesis (P^B) and irradiance (E) distributions and emprical relationships describing variability in light limited and light saturated carbon fixation (i.e.,the P^B vs E relationship)

1.9 Error sources for primary production estimates

There are two error sources for large scale primary production estimates:

1. Statistical errors resulting from undersampling, because estimates are based on finite data sets with limited spatial and temporal coverage; and

2. Methodological errors resulting from inaccuracies in observations made at a particular location.

Most analyses of primary productivity algorithm have focused strictly on methodological errors in satellite derived estimates by comparison with in situ measurements; however, in situ measurements also contain methodological errors. Methodological and statistical errors associated with both in situ measurements of primary production, as well as satellite data and usage must therefore be considered (Falkowski *et al.*, 1998).

It is generally assumed that methodological errors in in situ measurements are small compared with those of satellite-based algorithms. Based on this assumption, it has been shown that primary productivity algorithms can, at best, account for only 50-60 % of the total variance measured daily productivity. This error estimate is based on algorithms tested using in situ data only. When the added error incurred by using satellite data as input (e.g., inaccurate C_{sat} estimates) is taken into account, methodological errors associated with satellite algorithms will be larger (Falkowski *et al.*, 1998).

It is clear that uncertainties accumulate throughout the calculation of primary production, starting with that associated with the measurement of field parameters. Following Platt *et al.* (1988), $P^B{}_{max}$ and α^B cannot be known with a precision better than ±5% and ±20% respectively. In eccordance with the study of Balch *et al.* (1992) the error in the retrieval of surface chlorophyll from CZCS is 35%. Assuming all errors are independent, the resultant rms error on the computed water column primary production would be of the oder of 54% in open oceanic conditions. Approaching turbid waters in the near-shore areas, the error in retrieving chlorophyll concentration at the surface from space ranges from 50 to 100% or more increasing the error in the computed primary production to the order of 64 to 110%. Although the major steps in the computation were considered, such overall figures should be considered as lower estimates to retrieve primary production data from space (Hoepffner *et al.* 1999).

CHAPTER TWO
THE ADVANCED VERY HIGH RESOLUTION RADIOMETER

2. The Advanced Very High Resolution Radiometer

2.1 Introduction

The Advanced Very High Resolution Radiometer (AVHRR) is a broad band, four or five channel (depending on the model) scanner, sensing in the visible near infrared and thermal infrared portions of the electromagnetic (EM) spectrum. This sensor is carried on US National Oceanic and Atmospheric Administration's (NOAA) Polar Orbiting Environmental Satellites (POES) beginning with TIROS-N in 1978.

AVHRR was never designed for specifically or primarily for quantitative radiometric work. It was designed for use as an imaging radiometer, primarily for meteorological purposes.

The AVHRR sensor provides for global (pole to pole) on board collection of data from all spectral channels. Each pass of the satellite provides a 2399 km wide swath. The satellite orbits the earth 14 times each day at an altitude of 833 km above its surface. The Instantaneous Field of View (IFOV) of each channel is approximately 1.4 mr leading to a resolution at the satellite sub-point of 1.1 km.

AVHRR data are acquired in three formats:

- High Resolution Picture Transmission (HRPT) 1 km resolution
- Local Area Coverage (LAC) 1 km resolution
- Global Area Coverage (GAC) 4 km resolution

Table 2.1 Spectral bandwidths (nanometers) of the AVHRR

Channel #	TIROS-N	NOAA -6, -8, -10	NOAA –7, --9, -11, -12, -14	NOAA -13	IFOV (mr)
1	550-900	580-680	580-680	580-680	1.39
2	725-1100	725-1100	725-1100	7250-1000	1.41
3	3550-3930	3550-3930	3550-3930	3550-3930	1.51
4	10500-11500	10500-11500	10500-11300	10500-11300	1.41
5	Channel 4 repeated	Channel 4 repeated	11500-12500	11400-12400	1.30

HRPT data are full resolution image data transmitted to a ground station, as they are collected. LAC are also full resolution data but recorded with an on-board tape recorder for subsequent transmission during a station overpass. GAC data provide daily sub-sampled global coverage recorded on the tape recorders and then transmitted to a ground station.

In oceanography, the sensor has had primary importance for collecting data on sea surface temperature.

The AVHRR collects data in two reflected light bands: channel 1 in the red at 580-680 nm and channel 2 in the near infrared at 725-1100 nm. The red band is suitable for investigating turbid coastal waters and, fortuitously, has less sensitivity to dissolved pigments or chlorophyll than shorter wavelengths (blue or green). The near infrared band is used primarily for correction of atmospheric aerosols, the major contaminant in the signal (Stumpf & Frayer, 1997).

Table 2.2 Launch and service dates of TIROS-N and NOAA satellites

Satellite #	Launch	Service Dates	
TIROS-N	13/10/1978	19/10/1978	30/01/1980
NOAA-6	26/06/1979	27/06/1979	16/11/1986
NOAA-7	23/06/1981	24/08/1981	07/06/1986
NOAA-8	28/03/1983	03/05/1983	31/10/1985
NOAA-9	12/12/1984	25/02/1985	11/05/1994
NOAA-10	17/09/1986	17/11/1986	Present
NOAA-11	24/09/1988	08/11/1988	13/09/1994
NOAA-12	14/05/1991	14/05/1991	15/12/1994
NOAA-14	30/12/1994	30/12/1994	Present
NOAA-15	13/05/1998	13/05/1998	Present

2.2 Sea Surface Temperature Derivation from AVHRR

The most successful use of AVHRR data in oceanography is in the determination of sea surface temperature using data from the thermal infrared bands.

An overall view of the use of thermal infrared scanner data from a satellite for the determination of sea surface temperature (SST) is indicated in Fig. 2.1 (Cracknell, 1997). The left-hand side illustrates the physical processes involved. Radiation, which is emitted at the surface of the sea travels through the entire atmospheric column. It then reaches the satellite but during this travel its spectral distribution is significantly changed. The radiation arrives at the satellite and enters the objective aperture of the AVHRR. Eventually a signal is generated as 10 bit digital data. The right hand side outlines the processing operation where the digital data can be processed to retrieve the sea surface temperature on a pixel by pixel basis. The main steps involved are:

- Cloud detection and elimination
- Geometrical rectification
- Calibration of data (determination of brightness temperature)
- Conversion of satellite recorded radiance into water leaving radiance
- Conversion of water leaving radiance into sea surface temperature.

Now the calculation of SSTs is carried out routinely at a number of ground receiving stations around the world to produce charts or maps of SSTs on a regular basis at various spatial scales.

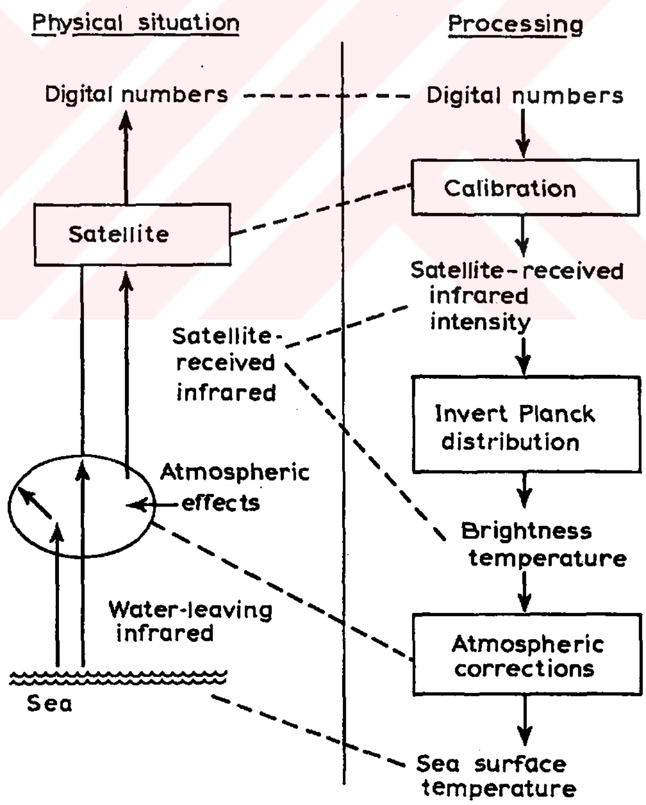

Figure 2.1 **Diagram to illustrate the determination of sea surface temperatures from satellite thermal infrared data (Cracknell, 1997).**

One of the algorithms used to derive sea surface temperatures from satellite thermal infrared data is the Multichannel Sea Surface Temperature Algorithm (MCSST) (Cracknell, 1997):

$$SST = a_1 + a_2T_4 + g(T_4\text{-}T_5) \tag{2.1}$$

Where,

a_1, a_2 =constants determined through a least squares fit to *in situ* data

g =weighing factor based on knowledge of absorption coefficients

T_4, T_5 =brightness temperatures as derived from channels 4 and 5

Sea surface temperature derivation from satellite provides the capability of further investigations on oceanographic and coastal processes. Ocean circulation studies involving the determination of flow patterns, fronts, eddies and rings and current vectors are based on processing the thermal infrared data from AVHRR. Geometrical rectification of the images is essential but atmospheric corrections are generally not necessary for ocean circulation studies.

2.3 Water Quality Parameters Derived from AVHRR

From a satellite, the studies of ocean colour are carried out by examining the amount of reflectance in the visible region of the electromagnetic spectrum. The visible wavelength channel of AVHRR (channel 1) is generally considered to be inappropriate for oceanographic applications because of its low radiometric sensitivity. The scanners that are generally used for ocean colour studies have visible bands that are more sensitive (Table 1.1). They also have a greater number of bands, which are necessarily narrower in wavelength range and which are able to be used in multi-spectral classification or in multi-channel algorithms for the determination of water parameters as suspended sediment and chlorophyll concentrations.

A particularly strong point in favor of the AVHRR, given the time scale on which oceanic conditions may change is the daily coverage (even twice a day if both the morning and afternoon satellites are used).

In channel 1 (covering wavelengths 580 to 680 nm, the orange and red) only about 10 percent of the signal received by the AVHRR originates from the water column, the atmosphere contributes the 90 percent. In channel 2 the contribution of the water column to the signal is negligible since the water molecules absorb the near infrared radiation. It is therefore extremely essential to try to calculate the atmospheric correction to channel 1 AVHRR data as accurately as possible. This concept will be discussed in detail in the next section.

CHAPTER THREE
MATERIALS AND METHODS FOR REMOTE SENSING OF SEA SURFACE REFLECTANCE IN IZMIR BAY

3. Materials and Methods for Remote Sensing of Sea Surface Reflectance in Izmir Bay

3.1 Introduction

Processing of AVHRR data for estimation of chlorophyll-a concentrations and attenuation coefficients in turbid coastal water requires three components:

(1) conversion of raw data to radiance;

(2) correction of satellite received radiance to water leaving reflectance;

(3) establishment of appropriate general models relating reflectance characteristics to materials in the water; and determination of the coefficients of the models appropriate for the area under study.

This section presents equations and procedures appropriate for this processing.

3.2 Study Area

Izmir Bay is situated on the western coast of the Anatolian peninsula, and is connected to the Aegean Sea. The bay is roughly "L" shaped with the leg of the "L" about 20 km wide and 40 km long and the base of the "L" about 5-7 km wide and 24 km long. From the standpoint of her topographical and hydrographical characteristics, Izmir Bay is considered as consisting of three regions among which outer bay is divided into further three sub-regions as shown in Figure 3.1.

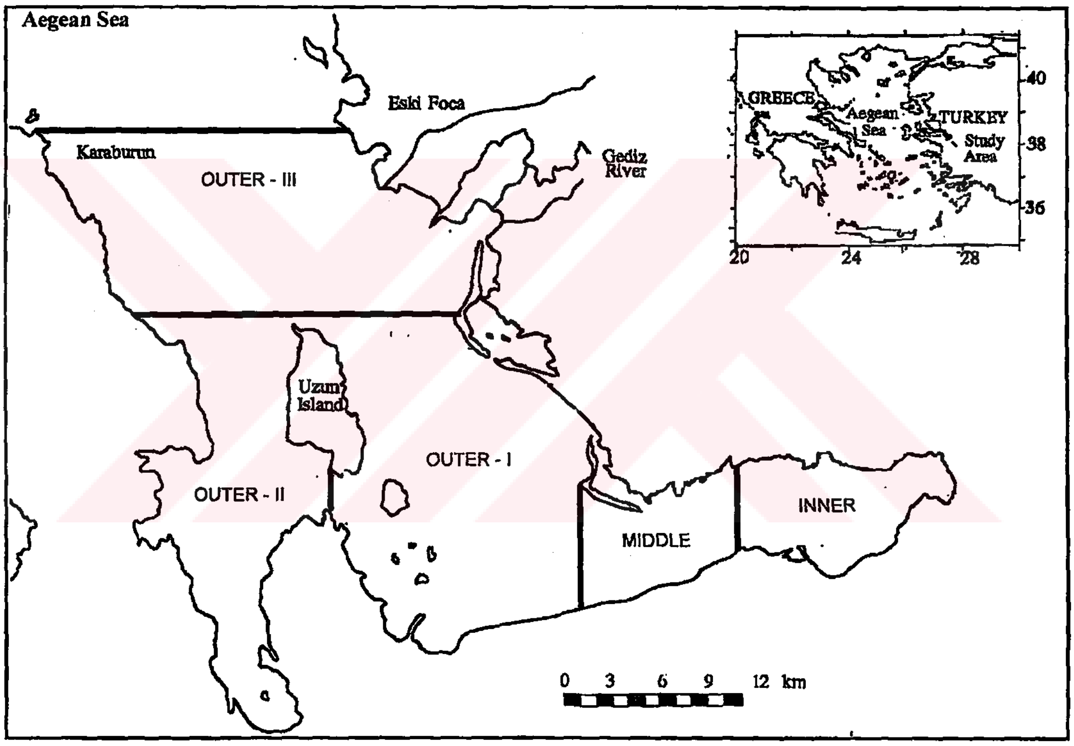

Figure 3.1 Study Area

The three sections of the Bay are distinguished by their different depth characteristics. The water depth of the Inner Bay ranges from 0 to 20 meters. The Middle Bay water depths range from 0 to 40 meters whereas the Outer Bay has relatively constant depth in the longitudinal direction ranging from 40 to 60 meters over an extension of 25 km.

Inner bay has been surrounded by the residential and industrial areas of Izmir, which is the third largest city in Turkey, and is also the gate between Turkey and

Europe as a significant industrial and commercial center with natural wealth and appropriate climatic conditions. Izmir Harbor - located in the well-protected innermost part of the bay - has always been an important nodal point of different transportation modes since 16th century (Akyarli *et al.*, 1997). Existence of a perfect natural port in the bay and topography of the land, easy access from the Anatolian hinterland, and ease of communications provoke the over-concentration of industrial plants at the vicinity of the bay.

Inputs creating pollution in the Izmir Bay consist of the following components: i) domestic waste waters produced by a population of nearly three million people; ii) industrial waste waters; iii) pollutant loads of Gediz river and other streams flowing into the bay; d) surface runoff; iv) agricultural drainage; v) port activities and sea traffic; vi) atmospheric input; vii) upflux from bottom sediments into the water column; viii) material transfer between the bay and the open sea (Akyarli *et al.*, 1997).

The characteristics of Izmir Bay as a receiving medium for wastewaters of well as the characteristics of pollutants discharged into the Bay can be summarized as follows:

- Izmir Bay, particularly the Inner Bay has a very limited waste assimilation and dilution capacity.

- Especially in the Inner Bay, the accumulation of mud at the mouths of streams and the high concentration of organic matter both in the sediments and in the water column has given rise to very negative results in this section from the point of view of smell and aesthetic appearance.

- Pollution inputs into the Bay have different weights according to their origins. Pre-treatment is obligatory and has been being applied to the industries. However, the continuous industrial discharges degraded the quality of the marine environment before the pre-treatment became obligatory. Domestic sources are mainly responsible for nutrient inputs.

- Besides the organic constituents that are directly disposed into the Bay at the present time, nitrogen and phosphorus contained in the wastewaters increases the primary productivity significantly. This phenomenon of secondary pollution augments the organic loads of the Bay especially in the inner sections.

Synthesis of data collected during several monitoring programmes - mostly conducted by IMST - shows that the Izmir Bay, especially the inner bay, is heavily polluted by nutrients, organic material - as a result of both primary and secondary productions - and coliform bacteria (Akyarli *et al.*, 1997).

3.3 Field Measurements

The dataset used in this study extends from June, 1996 to September, 1998. *In situ* data of physical, bio-chemical and biological parameters were collected in Izmir Bay from the eighteen oceanographic cruises of RV/Piri Reis associated with the Monitoring of the Izmir Bay Programme.

Analyses of chlorophyll-a (µg/lt) were carried out by filtering of samples on to glass fiber filters (Whatman GF/F) and by extraction in acetone. The measurements were carried out by the fluorometric methods (Strickland & Parsons, 1972). Beam attenuation was measured using a Seatech transmissometer (10 cm / 660 nm), fluorescence was measured by an underwater fluorometer (Chelsea Instruments) and secchi depth (m) measurements were selected from the database corresponding to the following stations in order to calibrate the AVHRR data with the *in situ* data.

Table 3.1. ***In situ* measurements used in the calibration study**

Date of *in situ* measurement			Station Codes																	
year	**month**	**day**	**002**	**003**	**006**	**009**	**010**	**011**	**013**	**015**	**016**	**017**	**020**	**021**	**023**	**024**	**027**	**042**	**043**	**Total**
1996	6	19									1		1	1	1	1	1			6
		20				1	1		1	1										4
	7	10			1	1	1	1	1			1	1	1		1	1			10
	10	7			1	1	1	1		1	1	1	1	1	1	1	1			12
1997	1	17				1				1	1	1	1	1	1	1	1			9
		18	1	1																2
		19						1	1											2
	6	11			1	1	1	1				1								5
		12							1	1	1		1	1	1		1			7
	7	3					1	1			1		1	1						5
	8	12											1				1			2
	9	22														1				1
		23											1	1			1			3
	10	2										1								1
	11	5											1	1	1	1				4
		7	1	1		1						1								4
1998	9	1				1						1								2
		2	1	1			1	1	1	1	1		1							8
Total			3	3	3	7	6	6	5	5	6	7	10	8	5	6	7			**87**

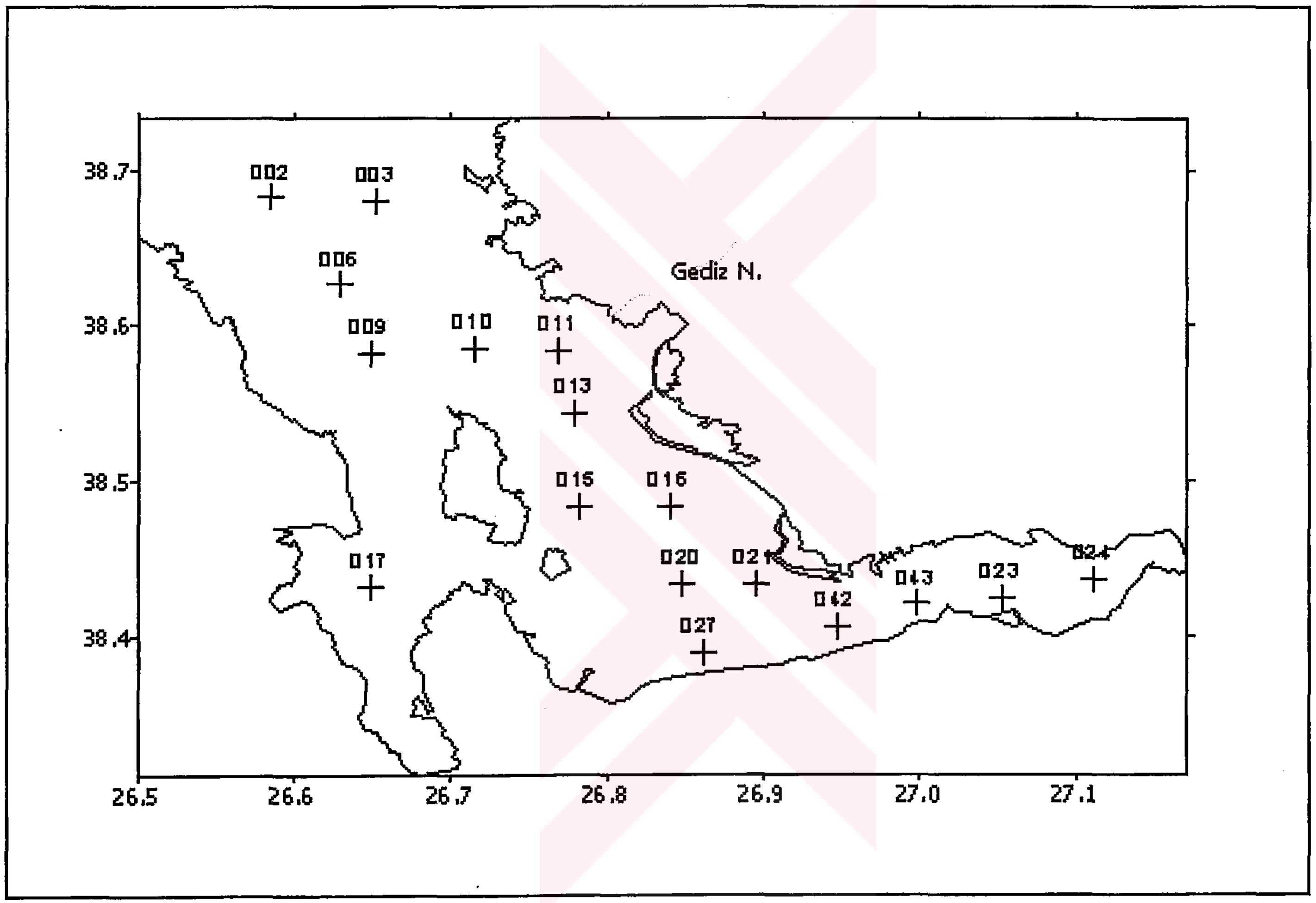

Figure 3.2 Selected Stations

3.4 Satellite imagery

The AVHRR raw data were received by the SMARTECH ground station of IMST (Fig. 3.3). Cloud-free scenes of AVHRR images that were corresponding to *in situ* measurement dates were selected in order to carry out a calibration study. Over a hundred images were examined and 18 cloud-free NOAA-14 images providing morning coverage were selected (Table 3.1). The subsets of Izmir Bay are extracted from the images. The visible (channel-1, 580-680 nm) and near-infrared (channel-2, 720-1000 nm) reflectance was processed as described in 3.4.1 and 3.4.2 and the imagery was remapped to a Clark/1988 projection with a pixel size of 1 km and residual navigational errors were removed by georeferencing them to the Turkey's digital shoreline. Pixels contaminated by land were not included in the analysis.

3.4.1 Conversion of Digital Numbers to Radiances for AVHRR

Rao & Chen (1996) post launch calibrations, which were developed for the Pathfinder program, were used here for the conversion of digital numbers to the satellite received radiances.

$$L(\lambda) = r^2 G(\lambda) [N(\lambda)-N_0(\lambda)] \quad (3.1)$$

$$r = 1-0.0167\cos(2\pi(J-3)/365) \quad (3.2)$$

$$G_1 = 0.0000690\, d + 0.566 \quad (3.3)$$

$$G_2 = 0.0000435\, d + 0.440 \quad (3.4)$$

Where

$G(\lambda)$ is the calibration slope, $N(\lambda)$ is the count value, $N_0(\lambda)$ is the count value corresponding to zero radiance (=41), r is the normalized distance from earth to sun, d is the days after launch (30 December 1994 for NOAA-14), and J is the Julian day (Stumpf *et al.*, 1997).

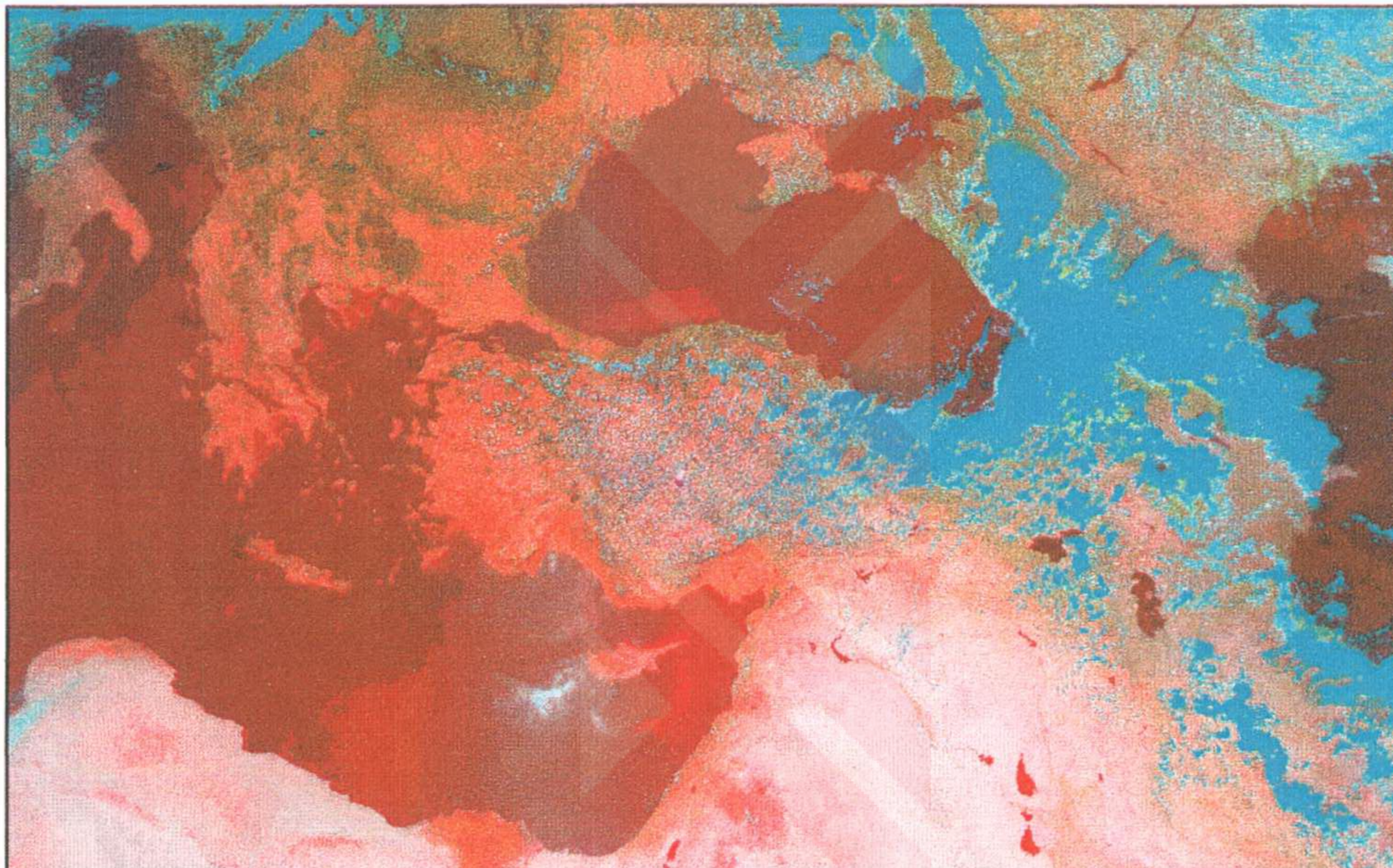

Figure 3.3 The AVHRR raw image which was received by the SMARTECH ground station of IMST (03.July.1997)

3.4.2 Atmospheric Corrections of AVHRR Data

The atmospheric correction studies on the AVHRR images were carried out by the Stumpf's (1992) algorithm in order to derive the water reflectance values. The reflectance of light from the water column (and bottom if shallow), R_w, can be found from

$$R_w = \frac{\pi L_w(\lambda)}{E_d(\lambda)} \tag{3.5}$$

$E_d (\lambda) = E_0 (\lambda) (1/r^2) \cos \theta\ T_0$

where L_w is the water leaving radiance, and E_d is the downwelling irradiance entering the water, E_0 is the solar constant (1628 for channel-1 and 1030 for channel-2 for NOAA-14), T_0 is the transmission through the atmosphere from the earth to the sun and λ is the spectral band. L_w and R_w refer to values above water surface, which may be called remote sensing reflectance. R_w is approximated by R_d, which is the Rayleigh and aerosol corrected channel 1 reflectance:

$$R_d = R_c(\lambda_1) - YR_c(\lambda_2) \tag{3.6}$$

with Y=1 and

$$R_c = \frac{\pi L_*(\lambda)/E_0(\lambda) - \pi L_r(\lambda)/E_0(\lambda)}{(1/r^2)T_0(\lambda)T_1(\lambda)\cos\theta_0} \tag{3.7}$$

where L_* is the radiance measured at the satellite , L_r is the Rayleigh radiance, E_0 is the solar constant, T_1 is the transmission through the atmosphere from the earth to the sensor.

T_0 and T_1 are estimated by:

$$T_0(\lambda) = \exp\left[-\left(\tau_r(\lambda)/2 + \tau_g(\lambda)\right)/\cos\theta_0\right] \tag{3.8}$$

$$T_1(\lambda) = \exp\left[-\left(\tau_r(\lambda)/2 + \tau_g(\lambda)\right)/\cos\theta_1\right] \tag{3.9}$$

where τ_r is the Rayleigh optical depth (0.056 for channel-1 and 0.022 for channel-2), τ_g is the gaseous absorption optical depth (i.e., for ozone and water vapor and is 0.035for channel-1 and 0.093 for channel-2), θ_0 is the solar zenith angle and θ_1 is the satellite zenith angle.

The Rayleigh radiance is found from:

$$L_r = \frac{E_0(1/r^2)\tau_r(\lambda)}{4\pi\cos\theta_1}\exp(-\tau_g(\lambda)/\cos\theta_1)\exp(-\tau_g(\lambda)/\cos\theta_0)(P(\psi_-)+0.052P(\psi_+)) \tag{3.10}$$

where the phase function is:

$$P(\psi_\pm) = (3/4)(1+\cos^2\psi_\pm) \tag{3.11}$$

and the scattering angles are:

$$\cos\psi_\pm = \pm\cos\theta_1\cos\theta_0 - \sin\theta_1\sin\theta_0\cos(\phi_1-\phi_0) \tag{3.12}$$

The solar zenith angle (θ_0) is the angle between the sun and the position's zenith. The solar azimuth angle (ϕ_0) is the position of the sun clockwise relative to the north. These can be computed from the Julian day (J), the time in GMT (T_{gmt}) for the point of interest, and the latitude (Φ) and longitude (Θ).

$$\cos\theta_0 = \sin\delta\sin\Phi + \cos\delta\cos\Phi\cos t_h \tag{3.13}$$

$$\cos\phi_0 = (\sin\delta\cos\Phi - \cos\delta\sin\Phi\cos t_h)/\cos(90^o - \theta_0) \tag{3.14}$$

where t_h is the solar hour angle, defined from solar noon:

$$t_h = (T_{local} - 12.00) * 15 * 2\pi) / 360 \quad (3.15)$$

$$T_{local} = T_{gmt} + (\Theta / 15) \quad (3.16)$$

for $t_h < 0$, (ϕ_0) is between 0-180°, for $t_h > 0$, (ϕ_0) is between 180-360°. The solar declination, δ, is estimated by:

$$\delta = 0.006918 - 0.399912 \cos \varepsilon + 0.070257 \sin \varepsilon - 0.006758 \cos 2\varepsilon + 0.000907 \sin 2\varepsilon$$

where $\varepsilon = 2\pi J/365$ (3.17)

The satellite azimuth angle is defined as clockwise from north, such that views east of nadir are less than 180°. For the AVHRR, this angle is approximated by the direction of the scanline. For the AVHRR, the satellite zenith angle can be found from:

$$\theta_1 = \arcsin (1.135 \sin \theta_v) \quad (3.18)$$

the view angle from the pixel n is:

$$\theta_v = 0.0541^\circ \,|1024\text{-}n| \quad (3.19)$$

All the processing was carried out in ERDAS software (version 8.3.1). The conversion and atmospheric correction algorithms were written in ERDAS Modeler which is presented in figure 3.4.

Table 3.2 List of NOAA-14 images and calibration parameters used in this study.

	DATE	JULIAN DAY	d	r	r^2
1	19.06.1996	171	537	1.0162	1.0326
2	20.06.1996	172	538	1.0163	1.0328
3	10.07.1996	192	558	1.0166	1.0335
4	07.10.1996	281	647	0.9988	0.9976
5	17.01.1997	17	749	0.9838	0.9678
6	18.01.1997	18	750	0.9839	0.9680
7	19.01.1997	19	751	0.9839	0.9681
8	11.06.1997	162	894	1.0154	1.0309
9	12.06.1997	163	895	1.0155	1.0312
10	03.07.1997	184	916	1.0167	1.0337
11	12.08.1997	224	956	1.0132	1.0265
12	22.09.1997	265	997	1.0034	1.0067
13	23.09.1997	266	998	1.0031	1.0062
14	02.10.1997	275	1007	1.0005	1.0010
15	05.11.1997	309	1041	0.9912	0.9825
16	07.11.1997	311	1043	0.9907	0.9815
17	01.09.1998	244	1341	1.0089	1.0179
18	02.09.1998	245	1342	1.0087	1.0174

(a)

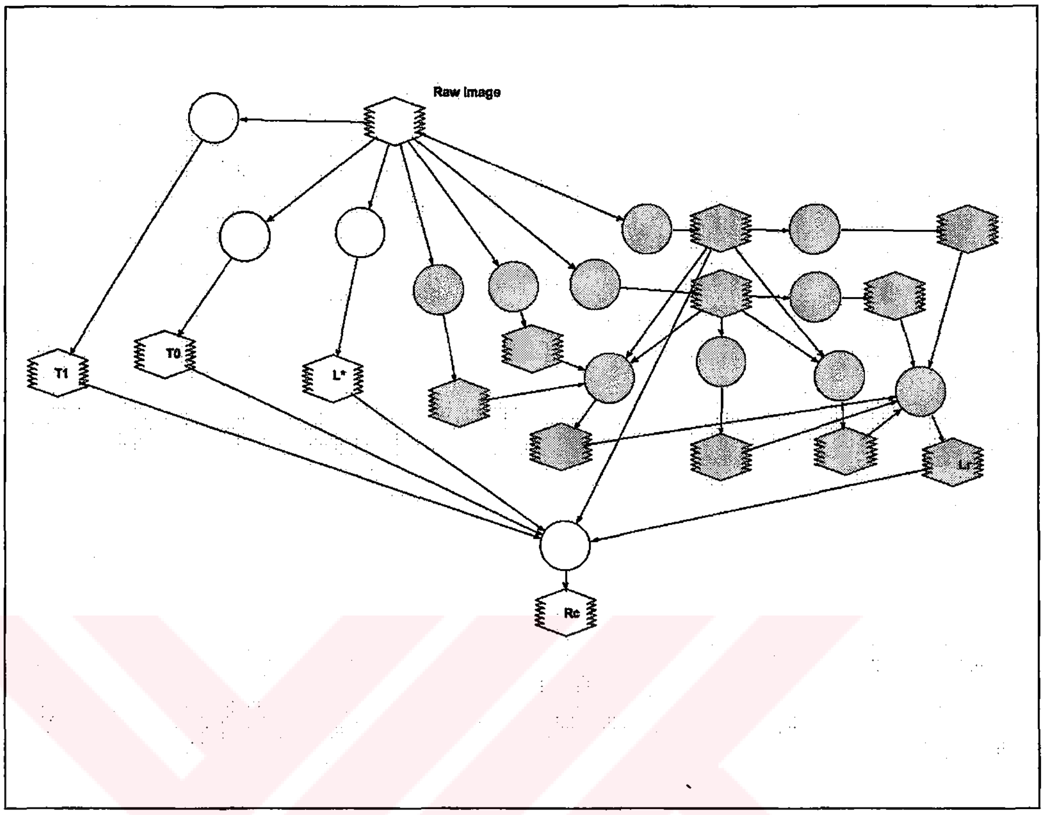

(b)

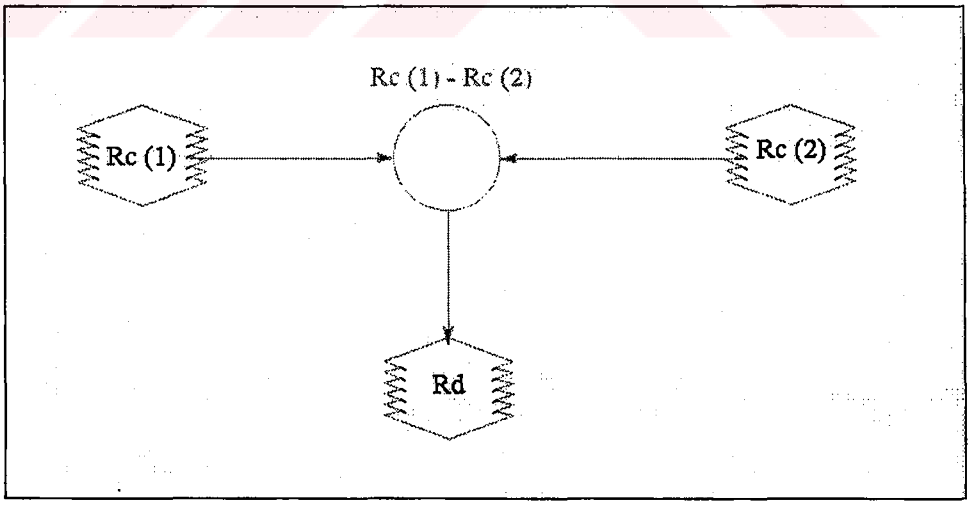

Figure 3.4 **The satellite image processing model which were written in ERDAS Modeler for this study (a) Conversion of DN to L_* (λ), calculation of $T_{1,\lambda}$,$T_{0,\lambda}$, L_r (λ) (gray boxes) and R_c (λ); (b) Calculation of R_d**

3.4.3 Calibration of AVHRR Reflectance Images

All empirical algorithms establish a relationship between optical measurements and the concentration of constituents based on experimental data sets, i.e. measurements of above or below surface reflectance (or radiance) spectra and coincident measurements of *in situ* concentrations (IOCCG No. 3, 2000).

All the data (both *in situ* and satellite driven reflectance) were stored in the database (FOXPRO environment) so that the queries and data matching processes have been easier.

The stations that were so close to the land have been omitted, as the reflectance values are not sensitive due to the land contamination.

Linear regression analyses were carried out in STATISTICA software.

Secchi Disc readings (m) are converted to Diffuse Attenuation Coefficients (m^{-1}) by the empirical relation:

$$K_d = f / S \qquad (1.12)$$

With f=1.4 for the inner and middle Bay and 1.7 in outer Bay (Gieskes, 1991).

CHAPTER FOUR
RESULTS OF THE CALIBRATION OF THE AVHRR SEA SURFACE REFLECTANCES

4. Results of the Calibration of the AVHRR Sea Surface Reflectances

4.1 Optical Water Quality Parameters of Izmir Bay

The optical properties of Izmir Bay is studied by analyzing the light transmission, Secchi depth, total suspended solids, fluorescence and chlorophyll-a measurements carried out between 1996-1998.

The *in vivo* fluorescence measurements had been grouped in two sets in accordance with the calibration of the fluorometer. Chlorophyll estimated from *in vivo* fluorescence and extracted in laboratory showed a strong linear relationship in each group (fig. 4.1). This allowed the recalculation of chlorophyll data by applying the calculated formula.

The following graphs (fig. 4.2, 4.3, 4.4) show that the concentration of chlorophyll-a is well correlated with the beam attenuation coefficient the Secchi depth readings and diffuse attenuation coefficient. This indicates that the bio-optical properties in Izmir Bay are dominated by the presence of the planktonic cells due to the high production. There is a significant correlation between TSS and diffuse attenuation coefficient for low chlorophyll-a concentrations (chl-a < $5mg.m^{-3}$, r^2=0.67) (fig. 4.5).

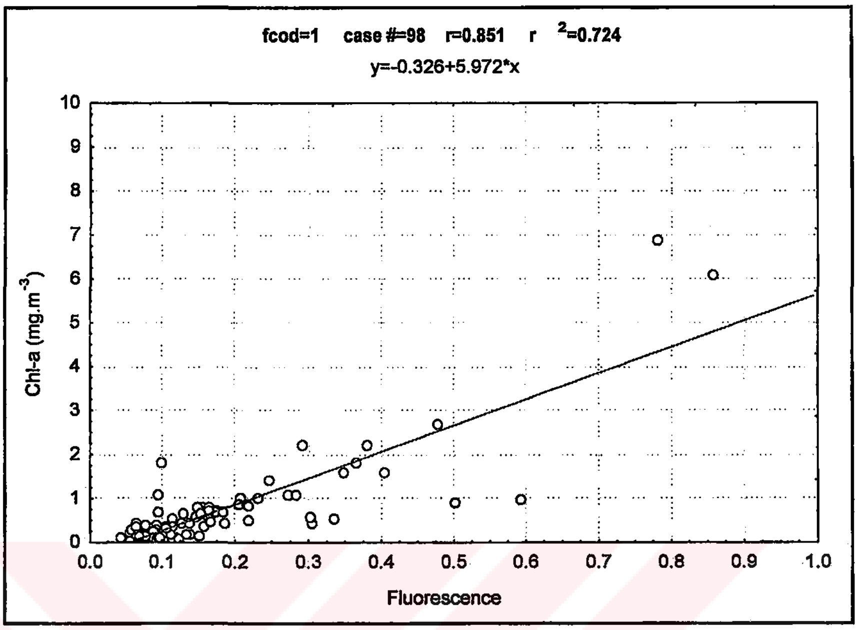

(a)

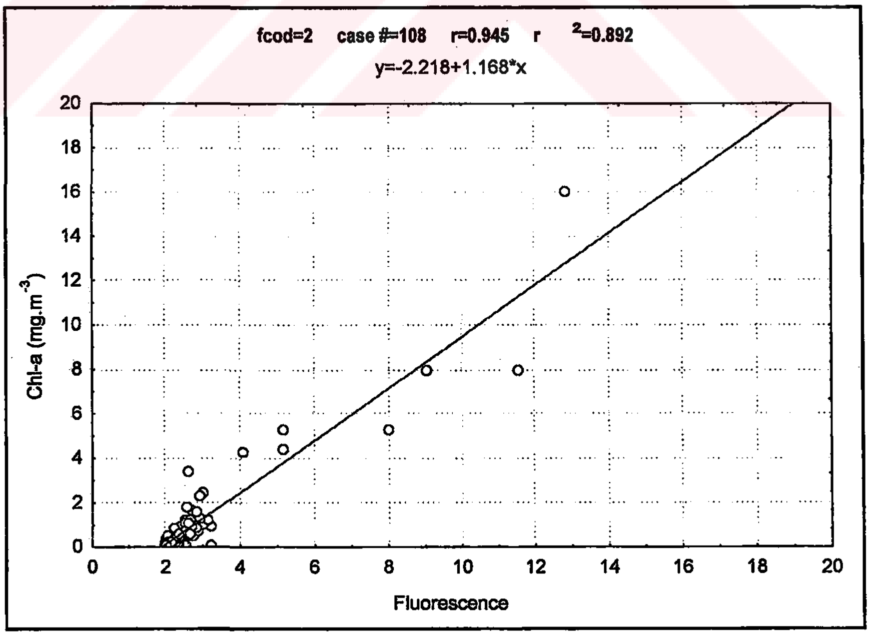

(b)

Figure 4.1 Relationship between *in vivo* fluoresence and chlorophyll-a measured in lab. (a) for group 1; (b) for group 2.

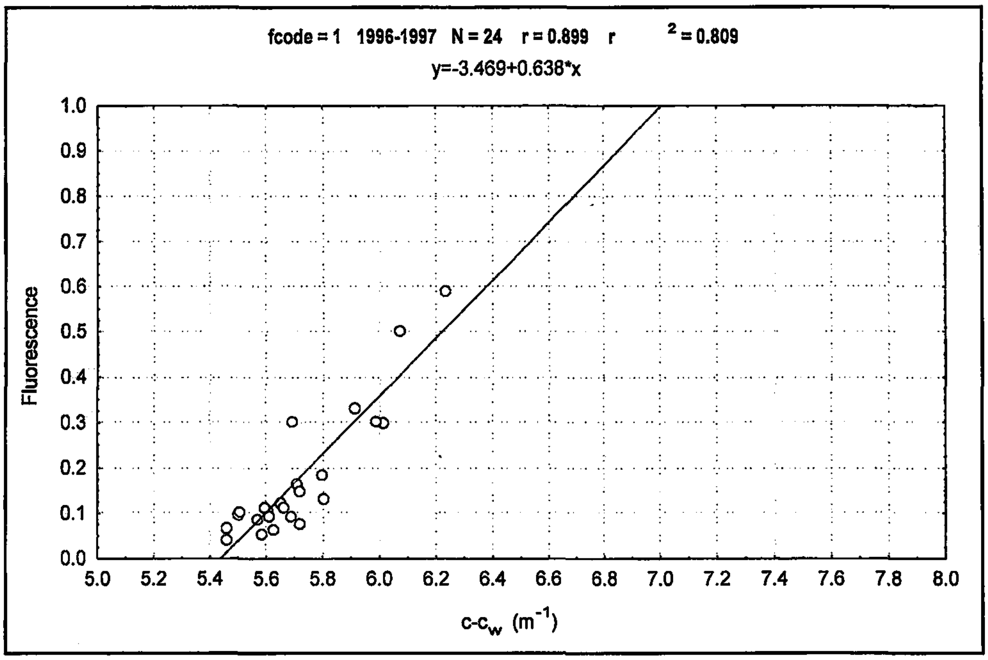

(a)

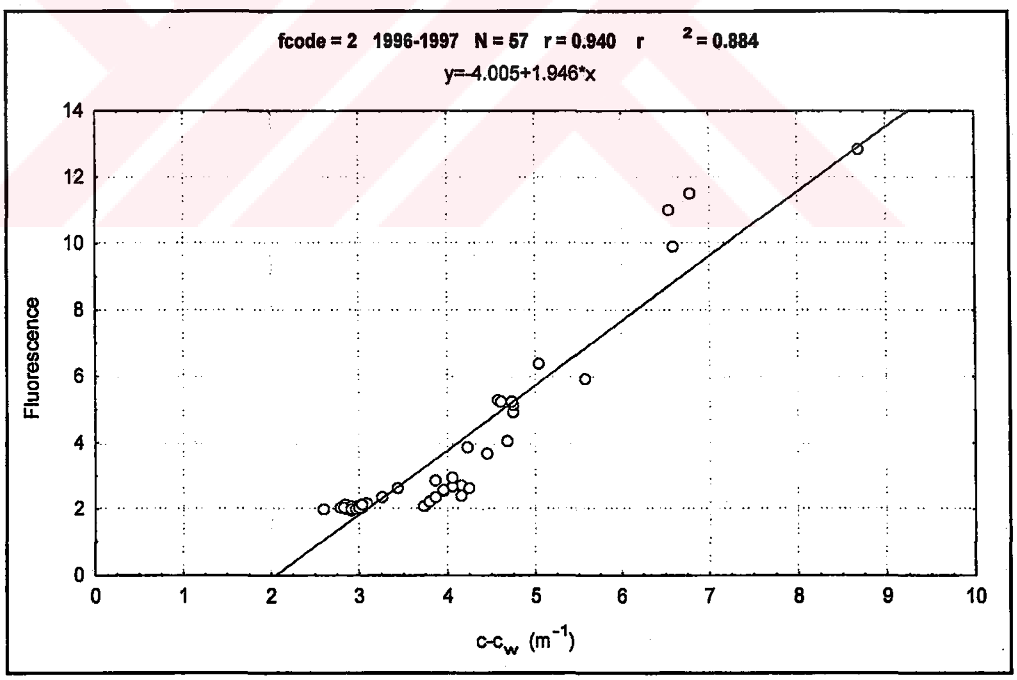

(b)

Figure 4.2 Relationship between *in vivo* fluoresence and c-c_w which is derived from beam transmittance (a) for group 1; (b) for group 2.

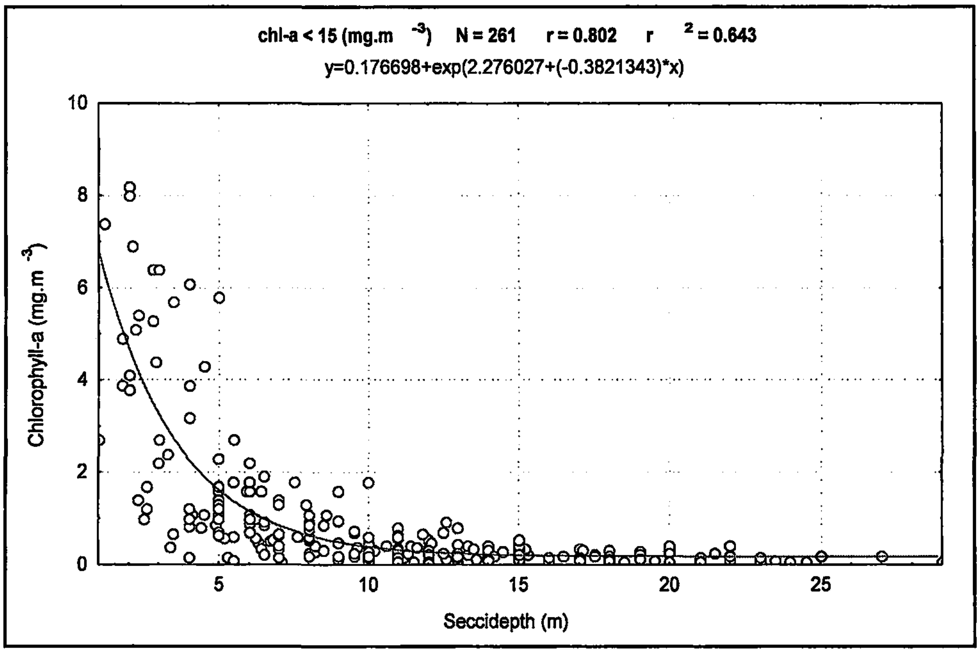

Figure 4.3 Relationship between *chlorophyll-a* and secchi depth readings

The indirect estimation of average extinction coefficient (diffuse attenuation coefficient), K_d is carried out from Secchi disk reading (SD) (Parsons *et al.*, 1984, Gieskes, 1991):

$K_d = 1.4 / SD$ for the inner and middle Bay

$K_d = 1.7 / SD$ for the outer Bay

Empirical relationships between light penetration and chlorophyll-a concentrations have been studied by several authors. One of the equations is derived from the actual field observations in the western North Atlantic by Riley, (1956) as follows (Parsons *et al.*, 1984):

$$K_d = 0.04 + 0.0088\ C + 0.054\ C^{2/3}$$

where K_d is the average extinction coefficient or the diffuse attenuation coefficient (m^{-1}) and C is the chlorophyll-a concentration ($mg.\ m^{-3}$). The constant 0.04 in this equation is close to the average extinction coefficient for visible light in clean water (0.0384) (Parsons *et al.*, 1984).

A similar non-linear model as above is compared with the linear model derived from *in situ* data for Izmir Bay. Figure 4.4 shows that the relationship between diffuse attenuation coefficient and chlorophyll-a concentrations does not vary much from one model to the other. In the non linear model the constant is given as 0.0384 and the other coefficients are calculated from the actual field data.

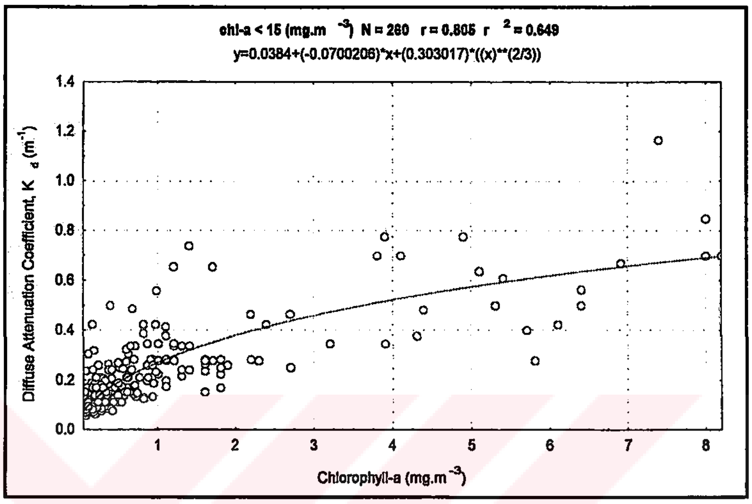

(a)

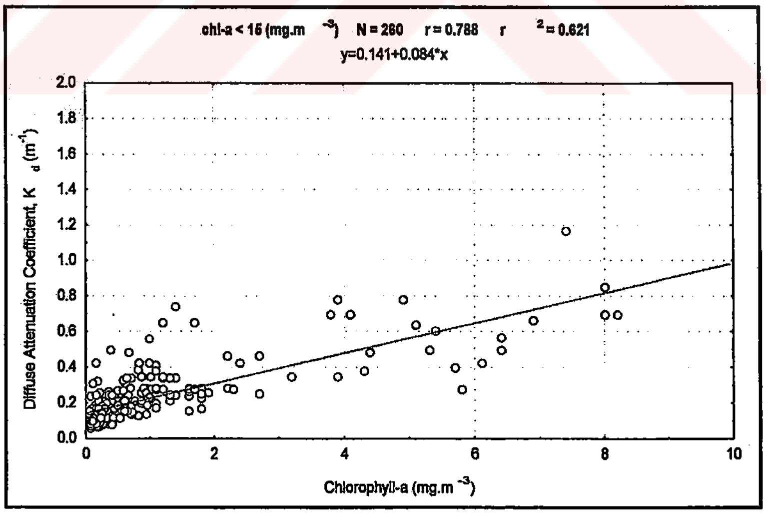

(b)

Figure 4.4 **Relationship between diffuse attenuation coefficient, K_d and chlorophyll-a (a) non linear estimation of K_d as a function of chlorophyll-a; (b) linear estimation of K_d as a function of chlorophyll-a.**

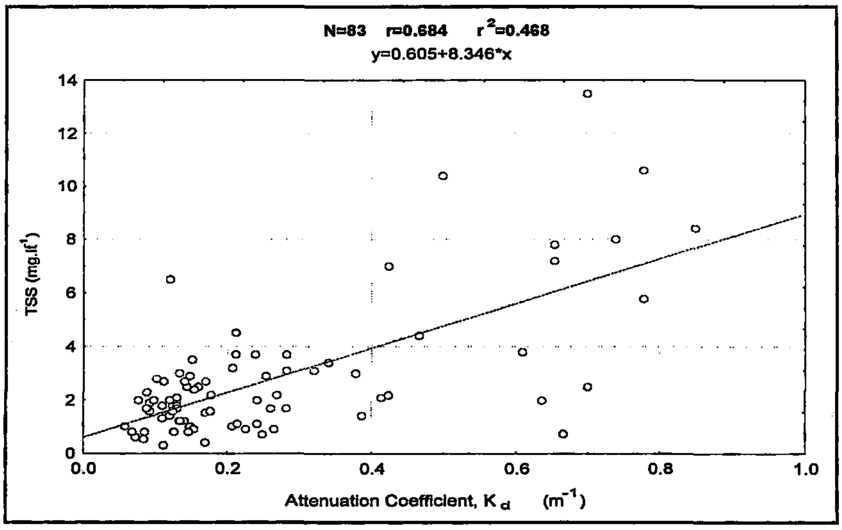

(a)

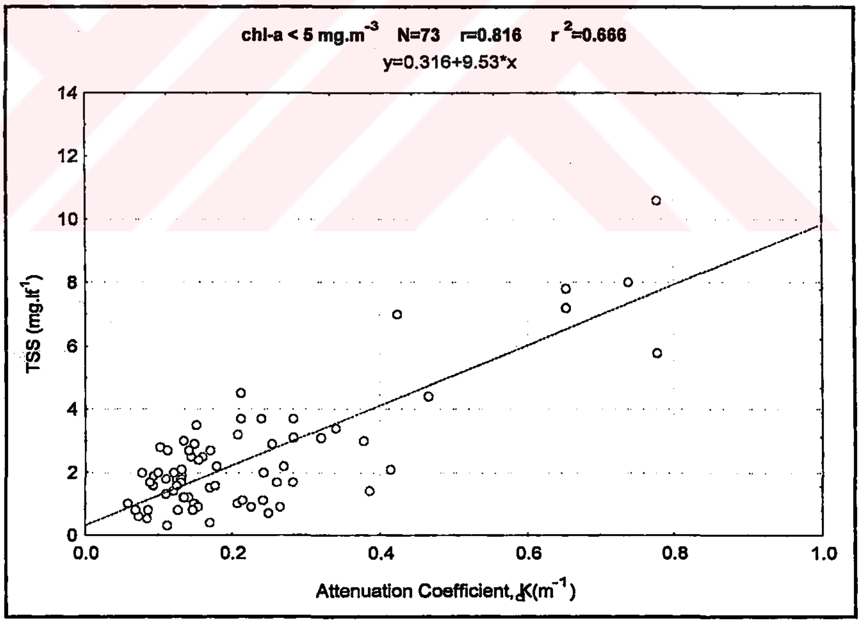

(b)

Figure 4.5 **Relationship between diffuse attenuation coefficient, K_d and total suspended solids, TSS (a) estimation covers all data; (b) estimation is bounded by the chlorophyll-a < 5 $mg.m^{-3}$.**

4.2 Reflectance and Temperatures of Sea Surface for Izmir Bay

The sea surface reflectance conversions were carried out as described in section 3.4 and the sea surface temperatures were derived by the SMARTECH's software that ran in ERDAS environment. MCSST (Multi Channel Sea Surface Temperature) Algorithm was used as described in section 2.2. The areal distribution of sea surface reflectance and temperatures were estimated by kriging the data (using Surfer 7.0 software package, Golden Software).

In all the scenes the northern part of the bay has relatively high reflectance in both winter and summer. This region is very shallow (below 5m). In shallow water the value for reflectance includes a component from the bottom (Stumpf & Frayer, 1997).

The reflectance of the Bay shows a seasonal variation with high levels in winter and low levels in the summer, corresponding to the seasonal variation in the winds and resuspension.

(a) (b)

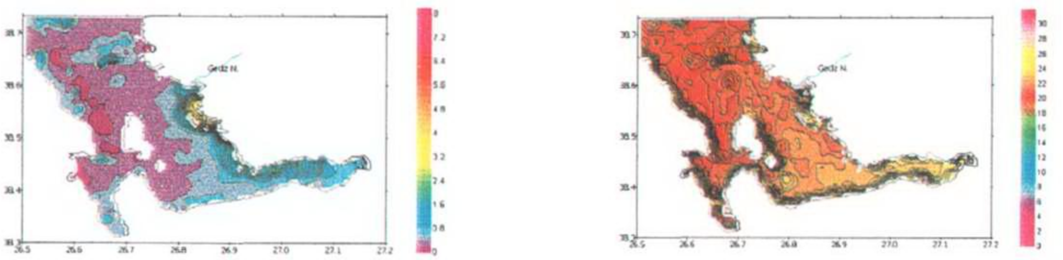

19.06.1996

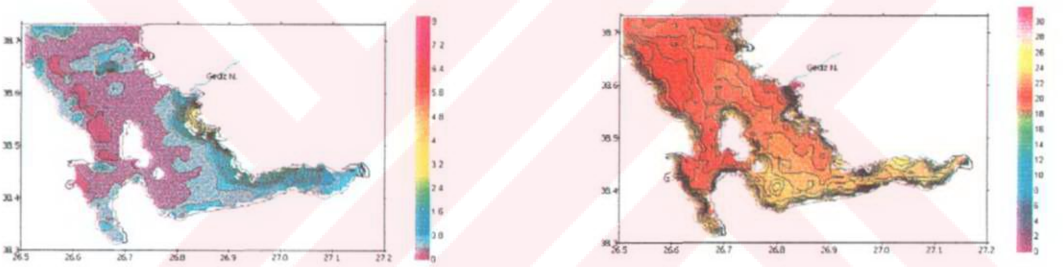

20.06.1996

Figure 4.6 (a) Reflectance and (b) Temperatures of Sea Surface for Izmir Bay (June 1996)

(a) (b)

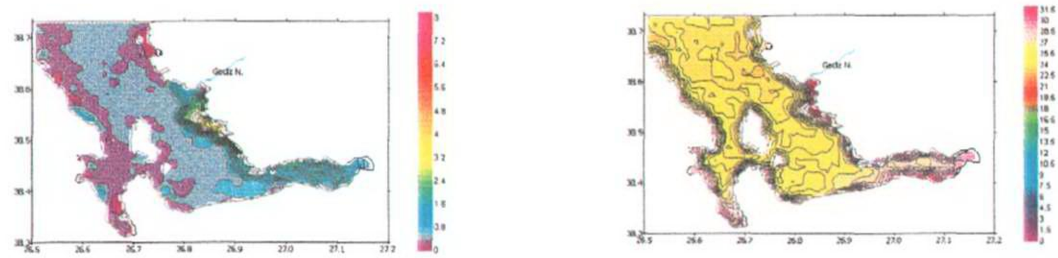

10.07.1996

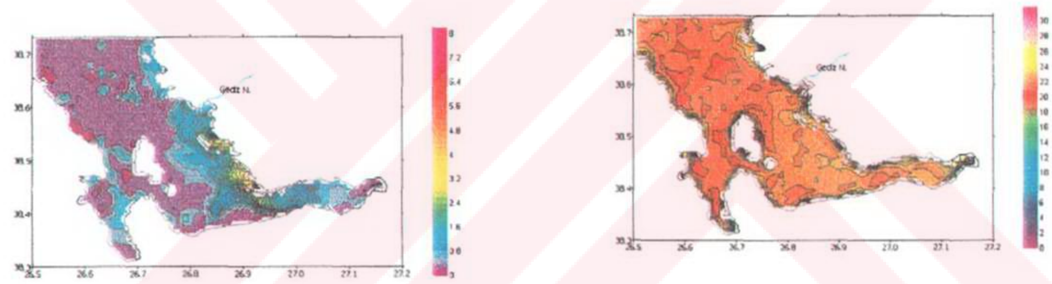

07.10.1996

Figure 4.7 (a) Reflectance and (b) Temperatures of Sea Surface for Izmir Bay (July and October 1996)

(a) (b)

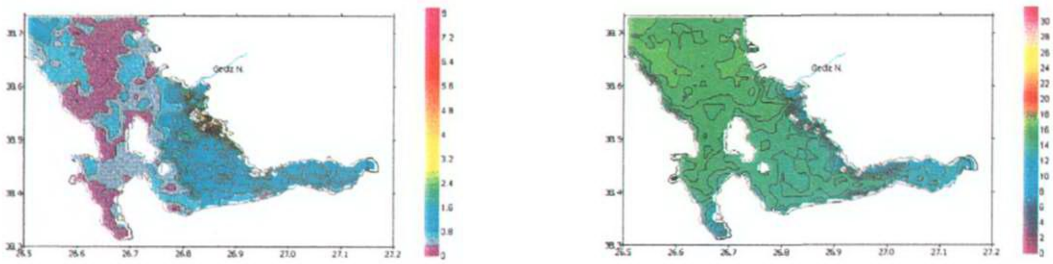

17.01.1997

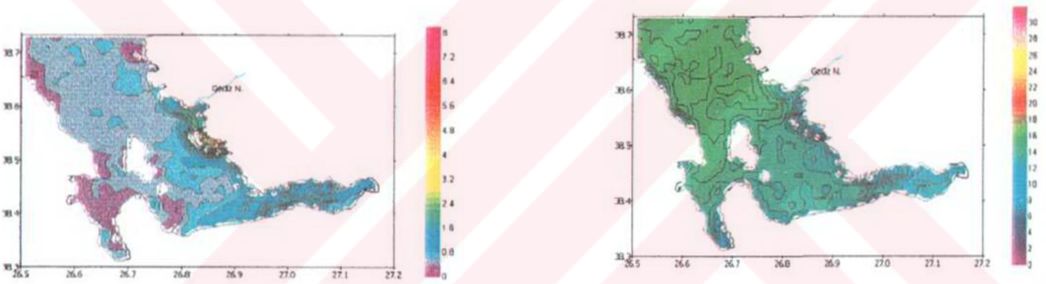

18.01.1997

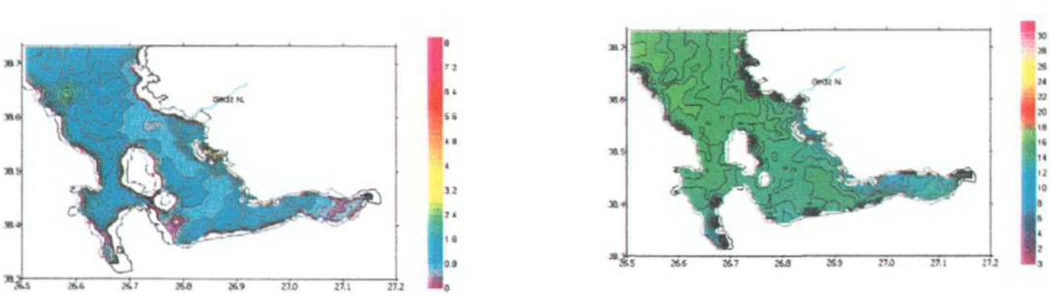

19.01.1997

Figure 4.8 (a) Reflectance and (b) Temperatures of Sea Surface for Izmir Bay (January 1997)

(a) (b)

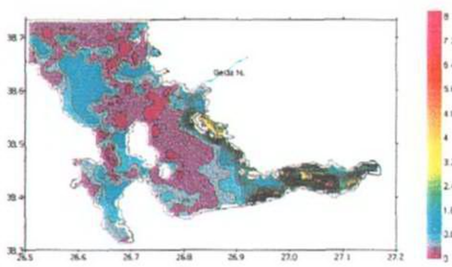

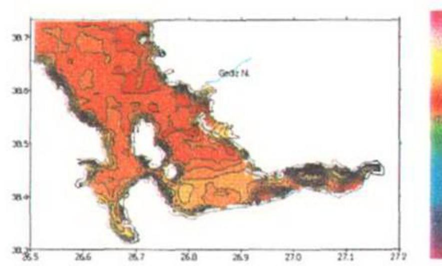

11.06.1997

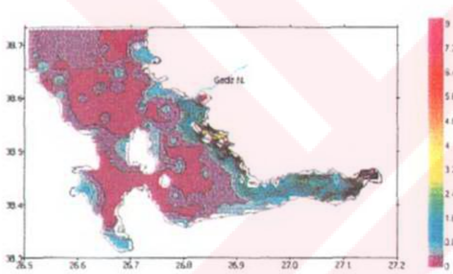

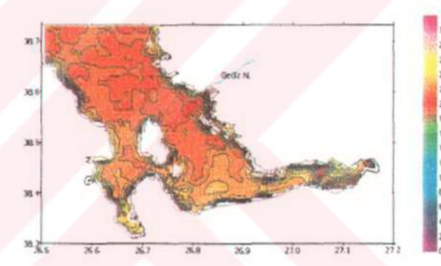

12.06.1997

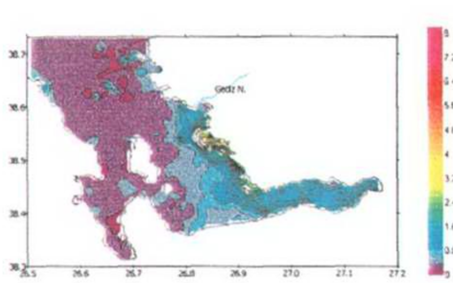

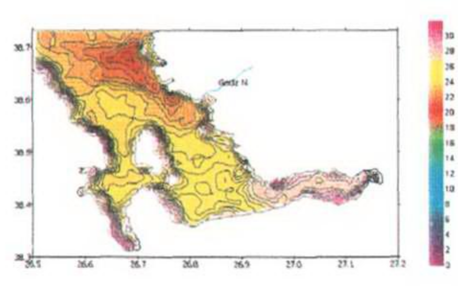

03.07.1997

Figure 4.9 (a) Reflectance and (b) Temperatures of Sea Surface for Izmir Bay (June and July 1997)

(a) (b)

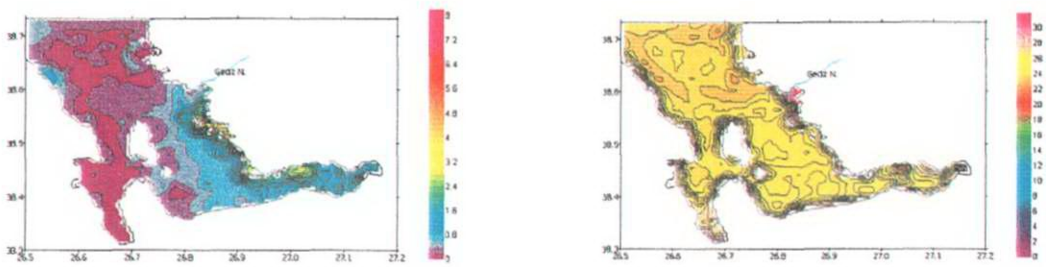

12.08.1997

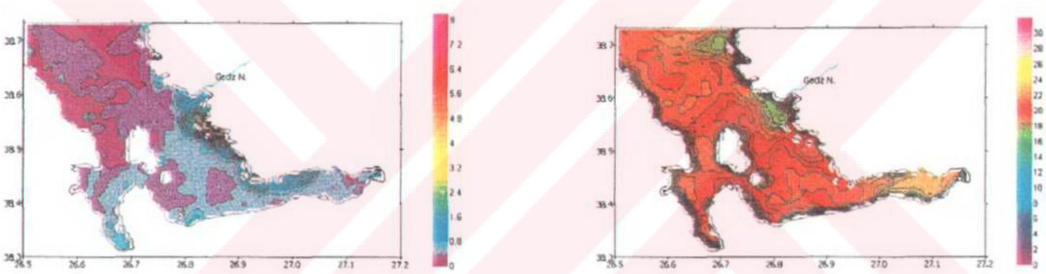

22.09.1997

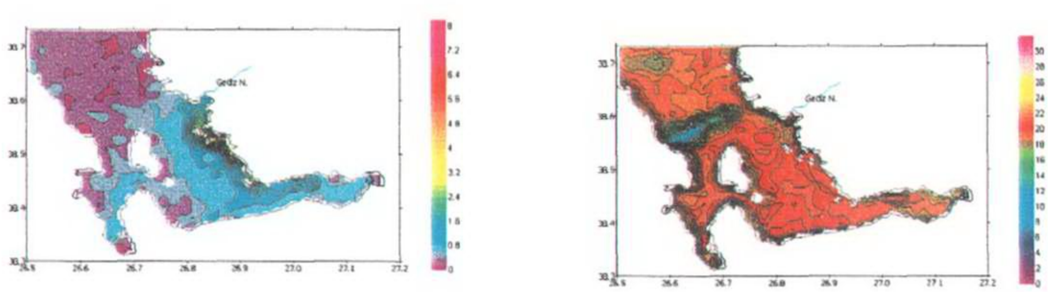

23.09.1997

Figure 4.10 (a) Reflectance and (b) Temperatures of Sea Surface for Izmir Bay (August and September 1997)

(a) (b)

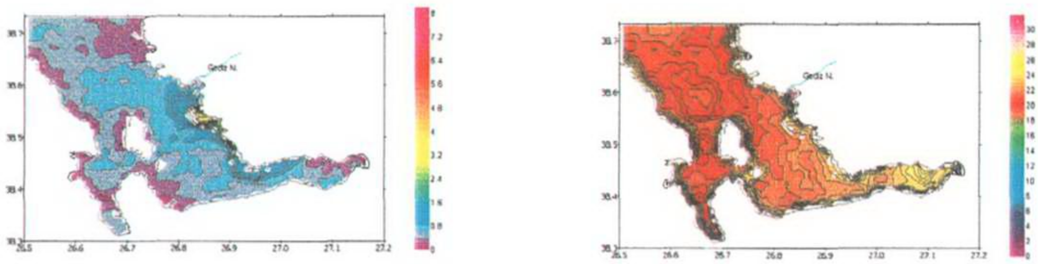

02.10.1997

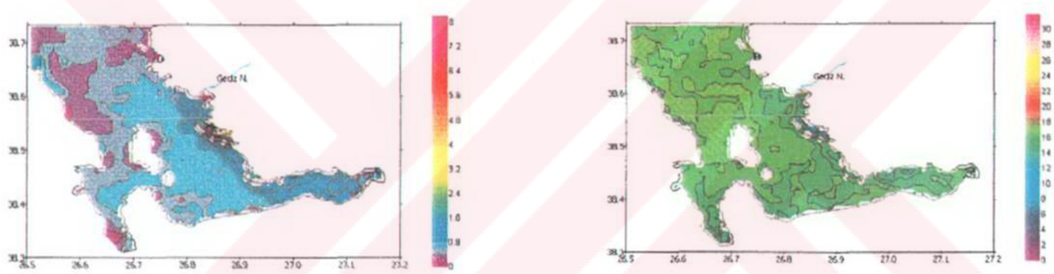

05.11.1997

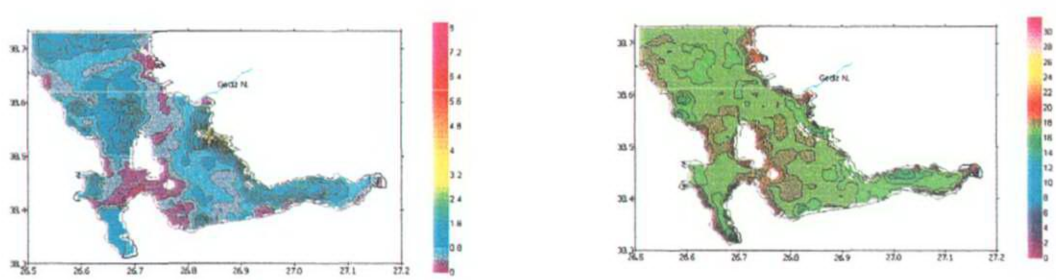

07.11.1997

Figure 4.11 (a) Reflectance and (b) Temperatures of Sea Surface for Izmir Bay (October and November 1997)

(a) (b)

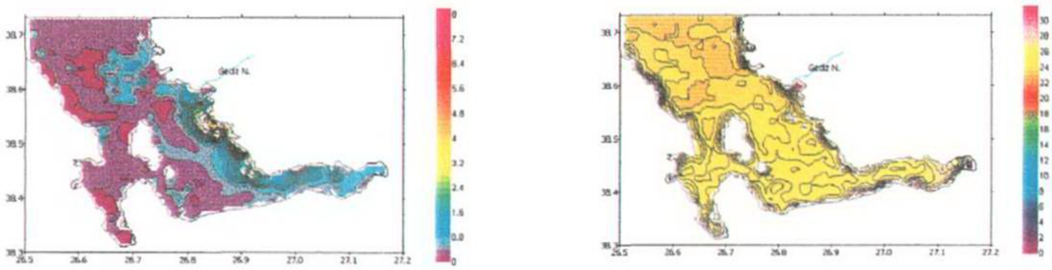

01.09.1998

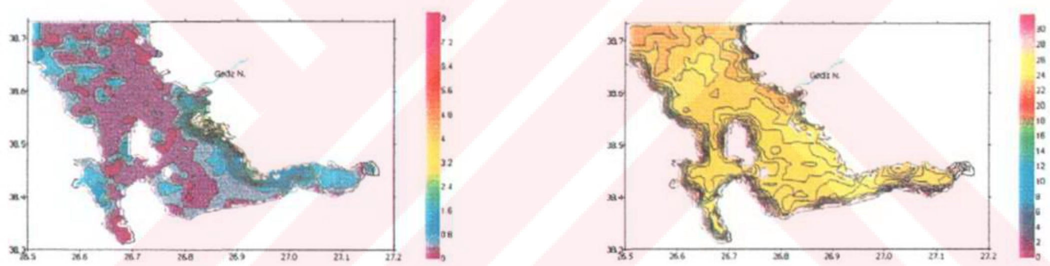

02.09.1998

Figure 4.12 (a) Reflectance and (b) Temperatures of Sea Surface for Izmir Bay (September 1998)

4.3 Calibration of Sea Surface Reflectances with Chlorophyll-a and Attenuation Coefficient

Chlorophyll-a is linearly correlated with sea surface reflectance for chl-a > 4mg.m^{-3} (fig. 4-13). The regression equation;

$$\text{Chl-a} = 26.705\text{-}17.447*\text{REF} \qquad ; \qquad r^2 = 0.715$$

fits the data of inner and middle parts of the bay where chlorophyll-a concentrations are generally higher. Eight data were excluded from the analysis for the validation purposes and the results of which are shown in Table 4.1.

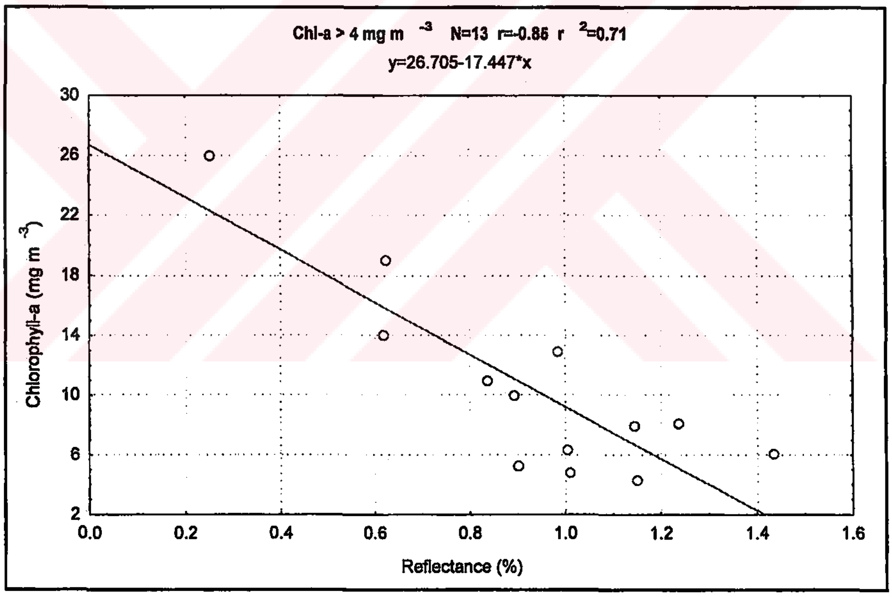

Figure 4.13 Relationship between chlorophyll-a and sea surface reflectance.

There is a nonlinear relation between the secchi disk depth and the sea surface reflectance (r=0.697) in Izmir Bay (fig. 4-14). TSS and sea surface reflectance are linearly correlated in the outer bay, for chl-a concentrations less than 5 mg.m^{-3} (fig. 4.15) indicating a scattering dominating system. Diffuse attenuation coefficient and sea surface reflectance are linearly correlated in the outer bay, for chl-a concentrations less than 4mg.m^{-3} (fig. 4.16).

Figure 4.17 shows the graphs of chlorophyll-a predicted from AVHRR versus chlorophyll-a measured in situ. The first graph shows the relation for all data, and the second one shows the relation when the data for 8.12.1997 was extracted.

Table 4.1 Comparison of predicted chlorophyll-a concentrations with the *in situ* measured ones.

Date: 7.10.1996 Station 23	Sea Surface Reflectance (%)	1.0090
	In situ Chl-a concentration ($mg.m^{-3}$)	4.4000
	Predicted Chl-a concentration ($mg.m^{-3}$)	9.1001
	-95.0 % Confidence Level	6.8798
	+95.0 % Confidence Level	11.3204
Date: 6.12.1997 Station 24	Sea Surface Reflectance (%)	0.6920
	In situ Chl-a concentration ($mg.m^{-3}$)	11.0000
	Predicted Chl-a concentration ($mg.m^{-3}$)	14.6309
	-95.0 % Confidence Level	11.8693
	+95.0 % Confidence Level	17.3926
Date: 8.12.1997 Station 24	Sea Surface Reflectance (%)	0.8300
	In situ Chl-a concentration ($mg.m^{-3}$)	22.0000
	Predicted Chl-a concentration ($mg.m^{-3}$)	12.2232
	-95.0 % Confidence Level	9.9577
	+95.0 % Confidence Level	14.4887
Date: 9.22.1997 Station 23	Sea Surface Reflectance (%)	0.6280
	In situ Chl-a concentration ($mg.m^{-3}$)	20.0000
	Predicted Chl-a concentration ($mg.m^{-3}$)	22.1717
	-95.0 % Confidence Level	16.8227
	+95.0 % Confidence Level	27.5207
Date9.02.1998 Station 42	Sea Surface Reflectance (%)	1.2360
	In situ Chl-a concentration ($mg.m^{-3}$)	4.4000
	Predicted Chl-a concentration ($mg.m^{-3}$)	5.1395
	-95.0 % Confidence Level	2.0413
	+95.0 % Confidence Level	8.2377
Date: 9.02.1998 Station 43	Sea Surface Reflectance (%)	0.759
	In situ Chl-a concentration ($mg.m^{-3}$)	8.0000
	Predicted Chl-a concentration ($mg.m^{-3}$)	13.4619
	-95.0 % Confidence Level	10.9797
	+95.0 % Confidence Level	15.9442
Date: 9.02.1998 Station 23	Sea Surface Reflectance (%)	1.0380
	In situ Chl-a concentration ($mg.m^{-3}$)	9.2000
	Predicted Chl-a concentration ($mg.m^{-3}$)	8.5941
	-95.0 % Confidence Level	6.3095
	+95.0 % Confidence Level	10.8787
Date: 9.02.1998 Station 24	Sea Surface Reflectance (%)	0.7790
	In situ Chl-a concentration ($mg.m^{-3}$)	15.0000
	Predicted Chl-a concentration ($mg.m^{-3}$)	13.1130
	-95.0 % Confidence Level	10.7011
	+95.0 % Confidence Level	15.5249

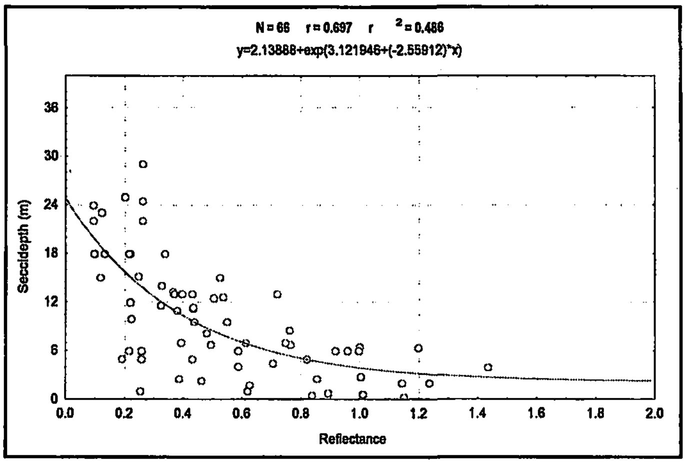

Figure 4.14 Relationship between secchi depth and sea surface reflectance

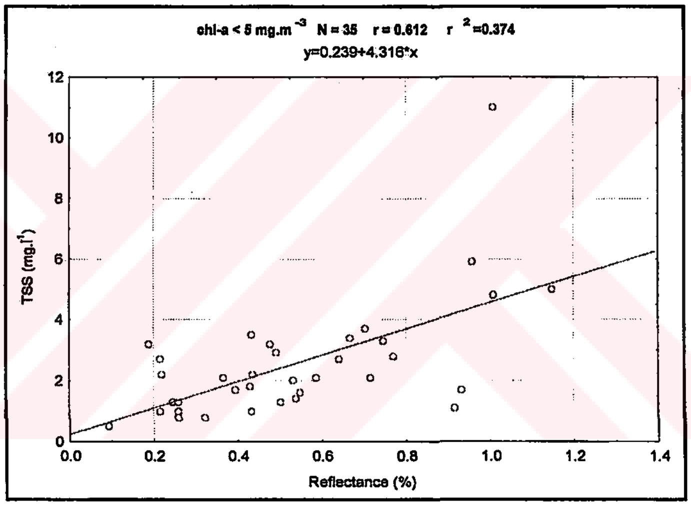

Figure 4.15 Relationship between TSS and sea surface reflectance

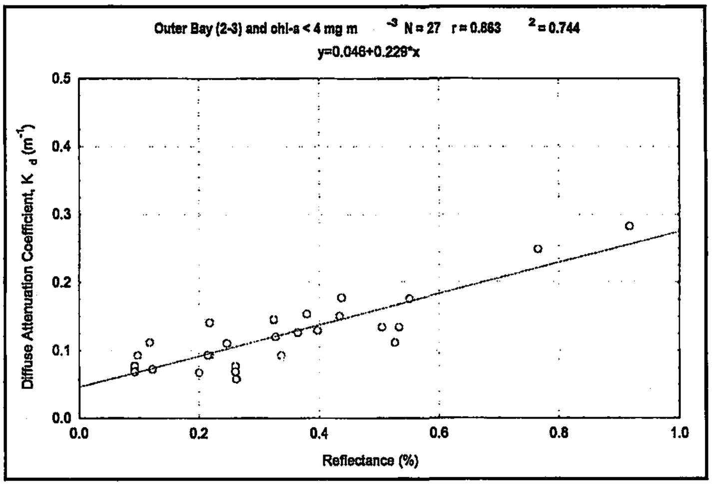

Figure 4.16 Relationship between diffuse attenuation coefficient, K_d and sea surface reflectance.

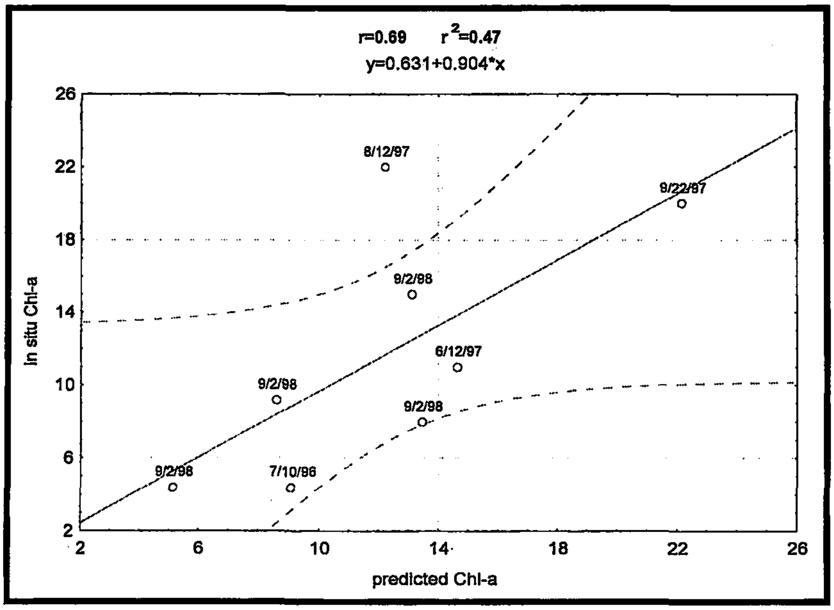

(a)

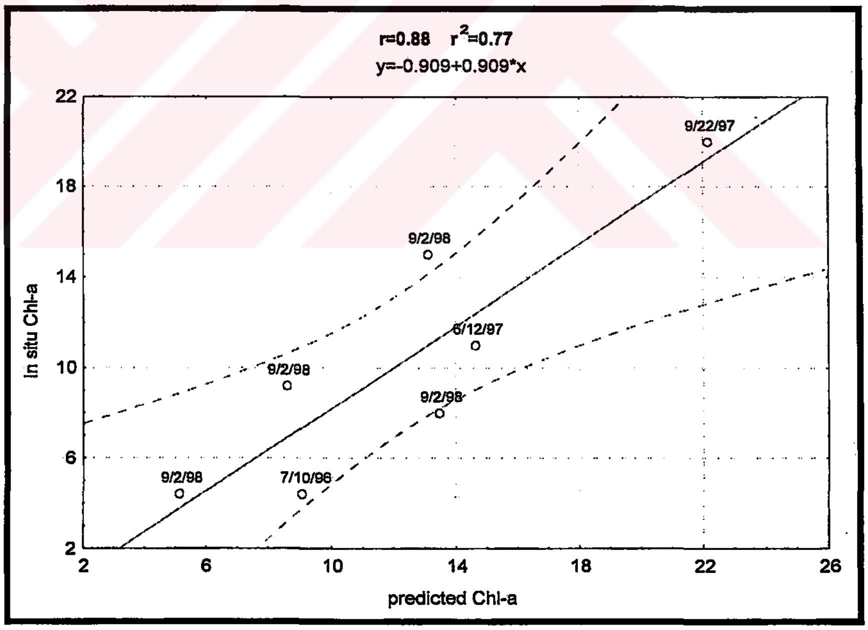

(b)

Figure 4.17 Chlorophyll-a predicted from AVHRR vs. Chlorophyll-a measured *in situ*. Dashed lines represents 95% confidence interval of the regression (a)shows the relation for all the validation points (b)shows the relation extracting the data for 8.12.1997.

CHAPTER FIVE
ESTIMATING PRIMARY PRODUCTION IN IZMIR BAY

5. Estimating Primary Production in Izmir Bay

5.1 Primary Production of Izmir Bay

Büyükışık *et al.* (1996) studied the ecological modeling of Izmir Bay with the field data of 1993. It was stated that the dominant species of winter were *Chaetoceros didymus*, *Chaetoceros decipiens, Thalassiosira gravida* and *Thalassiosira rotula*; during early spring *Gonyaulax sp., Scripsiella trochoideum;* and *Nitzschia pungens, Nitzschia closterium, Coscinosira polycorda* during late spring. *N. pungens, N. closterium, Gonyaulax sp.* were common during early summer; *Gyrodinium sp., Gymnodinium sp.*, during summer; *Eutreptiella gymnastica* during late summer whilst *Gyrodinium sp., S .trochoideum*, *Prorocentrum micans* and *Skeletonema costatum* were dominant species in autumn of 1993. In accordance with the studies carried out by Metin & Cirik (1999), Bizsel *et al.* (1997), Bizsel & Uslu (2000) and Bizsel *et al.* (2001) chl-a in the inner and middle bay varies from 4.46 to 24.61 mgm^{-3} on average for the period of May 1993- June 1994. Around the Harbor in the inner bay, the diatom population primarily consisted of *Skelotenema costatum* (about 54% and 93% of the total phytoplankton population in July 1993 and April 1994 respectively). The dinoflagellate *Scripsiella trochoidea* was the dominant species in July 1993 (about 73% of the total phytoplankton population), while *Prorocentrum micans* was the dominant species in April 1994 (about 42% of the total phytoplankton population) around the Pasaport region in the inner bay. The most striking result from these studies is that the phytoplankton composition changes rapidly in a short distance in the inner bay.

Primary production (PP) measurements have been performed by the scientists of Department of Hydrobiology of Ege University Water Products Faculty within the "Monitoring of the Izmir Bay Programme". PP measurements have been carried out at three locations (stations 24, 20, and 6) in Izmir Bay and light/dark bottle method have been used to derive the parameters of primary production model of Smith, 1965 and Vollenweider, 1965 (Marine Researches in Izmir Bay, 1998). The calculated values of those parameters and the PP amount for Station 24 in the inner bay have been given in Table 5.1. In Table 5.1 it is seen that assimilation index, P_{max}, varies from 4.4 to 25 mgC mg Chl^{-1} h^{-1}.

These studies show that the succession of phytoplankton species is very dynamic and interannual variability is so high in Izmir Bay. It is not possible to end up with a robust conclusion without the validation of estimated PP from empirical algorithms with in situ ^{14}C measurements.

In this study, primary production calculations were also carried out using the empirical approaches developed by Eppley et al. (1985) and Ryther & Yentsch (1957) as stated in Section 1.8. The regression equation given by Eppley et al. (1985) was selected as it is the simplest case and the method of Ryther & Yentsch (1957) was selected as there was a previous study on the primary productivity of Izmir Bay-, which was performed by Balcı et al. (1995) with the same method. The results of the calculations were shown in Table 5.2. As an initial estimate, Ryther and Yentsch (1957) assigned P^b_{opt} a constant value of 3.7 mgC $(mgChl)^{-1}$ h^{-1}, which Cullen (1990) suggested should be revised to 4.8 mgC $(mgChl)^{-1}$ h^{-1} due to improvements in the determination of pigment concentrations (Behrenfeld & Falkowski, 1997). So PP estimation from the method of Ryther & Yentsch (1957) for Izmir Bay was carried out both by taking P^b_{op} as 3.7 mgC $(mgChl)^{-1}$ h^{-1}, the results of which were given in column indicated as (1) and by taking P^b_{op} as 4.87 mgC $(mgChl)^{-1}$ h^{-1}, the results of which were given in column indicated as (2).

Table 5.1 Annual Primary Production calculations and its parameters for Station 24 (Marine Researches in Izmir Bay, 1998).

	P_{max} (mgC/mgChl-a/hr)	I_k (ft-cd)	PP (mgC/m^2/day)	K_d (m^{-1})	Chl-a (mg/m^3)	POC (mg/m^3)
January 1997	9	560	3322	0.229	4.64	2519
May 1997	25	500	23386	0.4	6.45	-
June 1997	-	2400	1419	0.32	2.88	2276
August 1997	4.4	200	5256	0.30	0.64	3088
November 1997		800	3546	0.43	n.d	1519
September 1998		500	5010	1.107	7.04	1995

Table 5.2 Primary Production calculations and its parameters for Station 24 using empirical approaches.

	I_o* (gcal/m^2)	Chl-a (mg.m^{-3})	K_d (m^{-1})	R* (rel. units)	PP (mgC/m^2/day) (1)	(2)	(3)
January 1997	261.6	8.2	0.70	15.1712	657.56	853.05	2863.56
June 1997	646.9	11	0.70	25.6884	1493.60	1937.64	3316.62
August 1997	536.7	22	1.40	22.8808	1330.36	1725.87	4690.42
November 1997	294.2	4.9	0.52	16.2144	566.94	735.49	2213.59
September 1998	550.05	15	1.08	23.2008	1195.67	1551.14	3872.98

* Parameters of PP in the equation of Ryther & Yentsch, 1957

(1) PP calculated by the method of Ryther & Yentsch, 1957 with p = 3.7 mgC mgChl^{-1} h^{-1}

(2) PP calculated by the method of Ryther & Yentsch, 1957 with p = 4.8 mgC mgChl^{-1} h^{-1}

(3) PP calculated by the method of Eppley *et al.*, 1985

The surface radiation intensity, I_o in Table 5.2 was obtained from Guzelyali Meteorological Station. The chlorophyll-a values in Table 5.2 were measured by the staff of IMST as stated in section 3.3. They are much higher than the values stated in Table 5.1. This may be due to different sampling and measurement methods.

The distributions of *in situ* chlorophyll-a concentrations in Izmir Bay and the chlorophyll-a concentrations which were retrieved from NOAA images for the inner bay are shown in Figures 5.1-5.5. The predicted chlorophyll-a values were used in the estimation of primary production in Izmir Bay and the results were shown in Table 5.3.

Table 5.3 Remotely estimated primary production in Izmir Bay

date	Reflectance (%)	chl-a ($mg.m^{-3}$)	PP(1) ($mgC/m^2/day$)	PP(2) ($mgC/m^2/day$)	PP(3) ($mgC/m^2/day$)
17.01.1997	1.2370	5.1231	410.82	532.96	2263.4180
12.06.1997	0.6920	14.6317	1986.71	2577.36	3825.1374
12.08.1997	0.8300	12.2240	739.19	958.95	3496.2823
05.11.1997	1.0100	9.0835	1050.98	1363.43	3013.8895
02.09.1998	0.6340	15.6436	1246.97	1617.69	3955.1994

(1) PP calculated by the method of Ryther & Yentsch, 1957 with p = 3.7 mgC $mgChl^{-1}$ h^{-1}

(2) PP calculated by the method of Ryther & Yentsch, 1957 with p = 4.8 mgC $mgChl^{-1}$ h^{-1}

(3) PP calculated by the method of Eppley *et al.*, 1985

Balcı *et al.* (1995) estimated primary production in Izmir Bay by the method of Ryther & Yentsch, (1957) with p = 3.7 mgC $mgChl^{-1}$ h^{-1}, and found that the primary production in the inner bay was between 135-1455 ($mgC/m^2/day$) for the period of February, 1990-December, 1992.

(a)

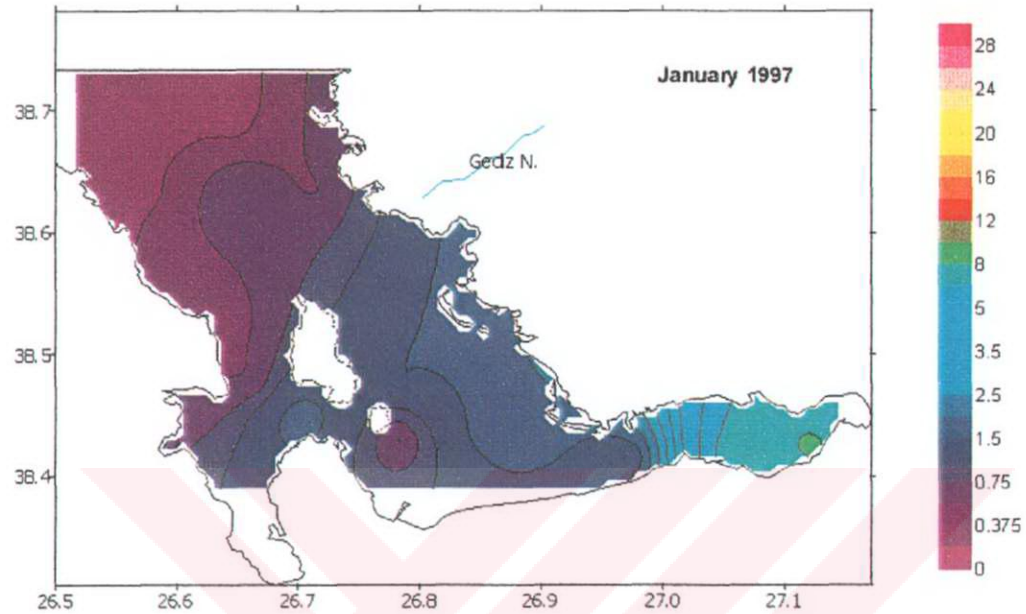

(b)

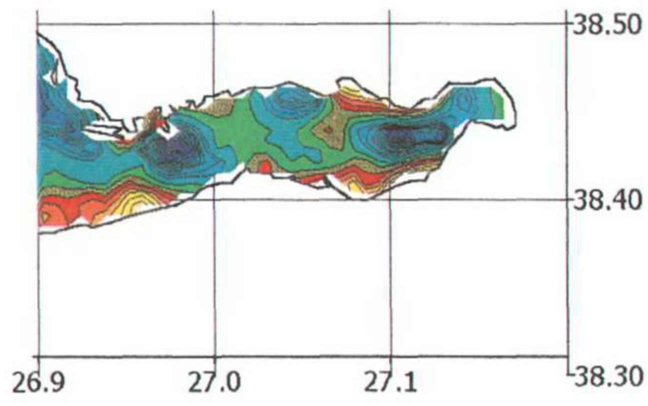

Figure 5.1 The distributions of (a) *in situ* chlorophyll-a concentrations in Izmir Bay and (b) the chlorophyll-a concentrations which were retrieved from NOAA images for the inner bay (January 1997)

(a)

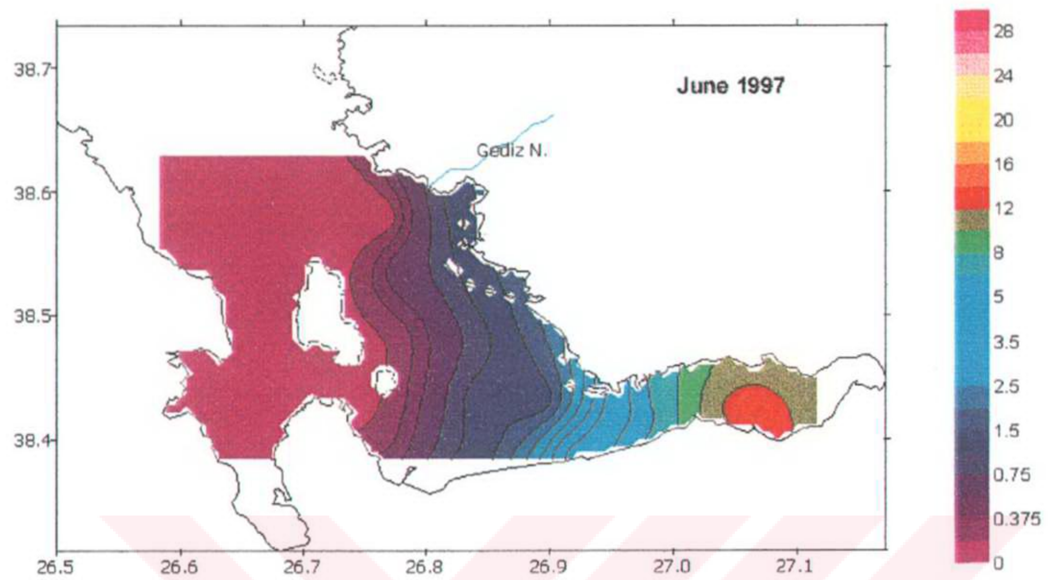

(b)

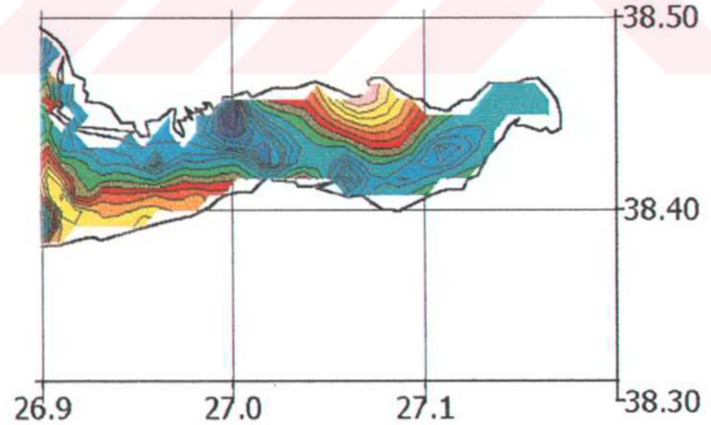

Figure 5.2 The distributions of (a) *in situ* chlorophyll-a concentrations in Izmir Bay and (b) the chlorophyll-a concentrations which were retrieved from NOAA images for the inner bay (June 1997)

(a)

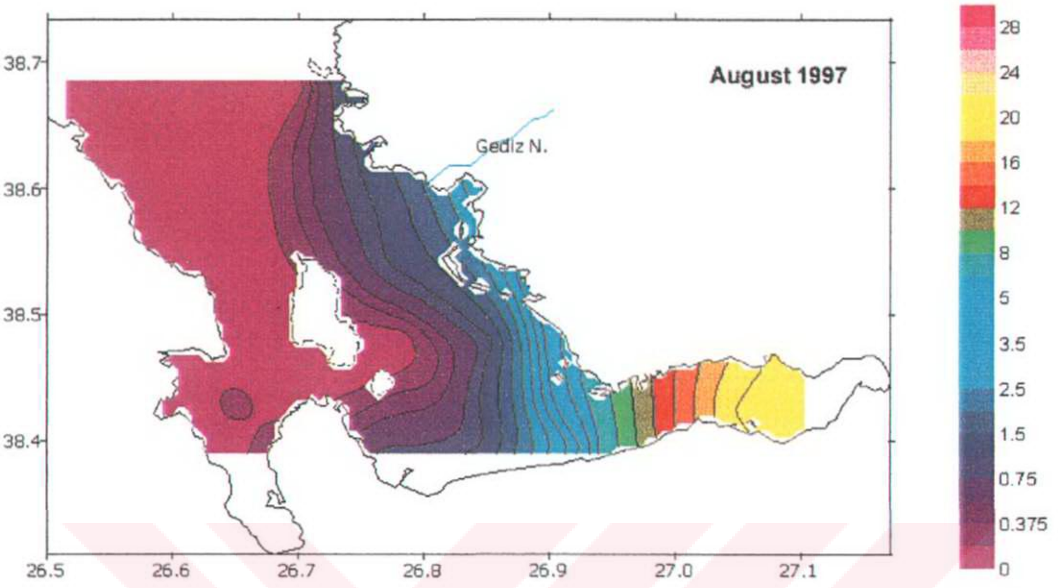

(b)

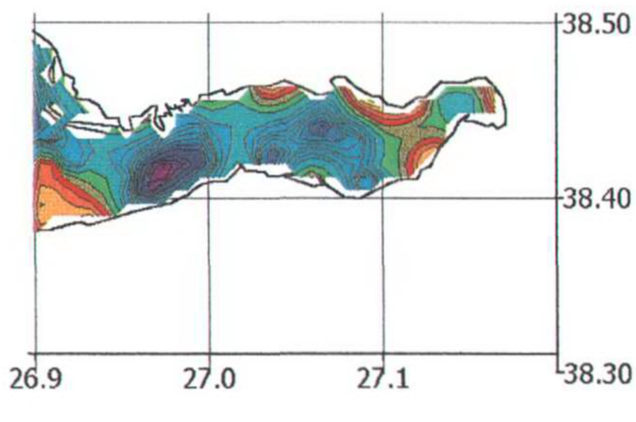

Figure 5.3 The distributions of (a) *in situ* chlorophyll-a concentrations in Izmir Bay and (b) the chlorophyll-a concentrations which were retrieved from NOAA images for the inner bay (August 1997)

(a)

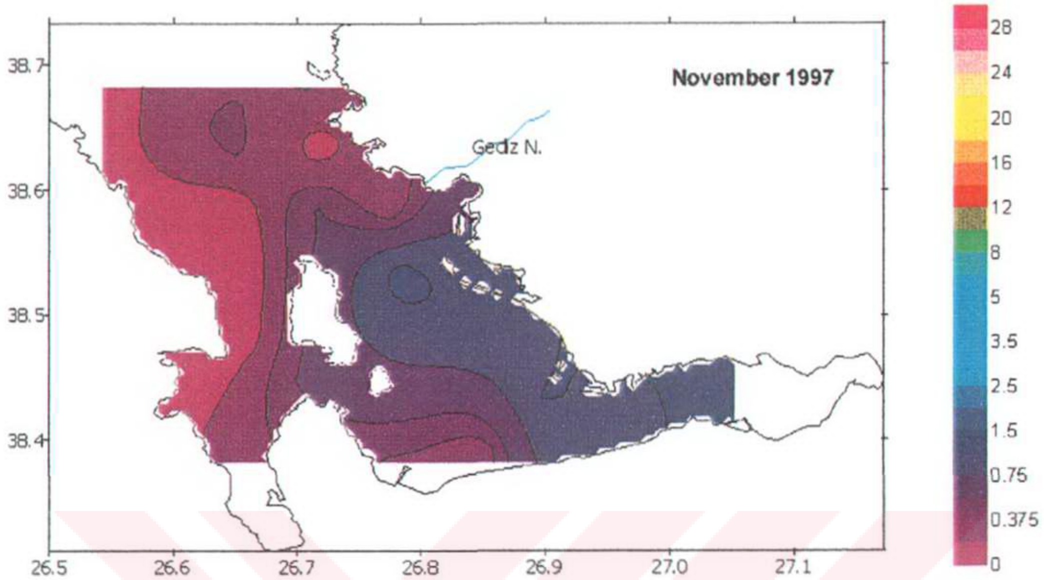

(b)

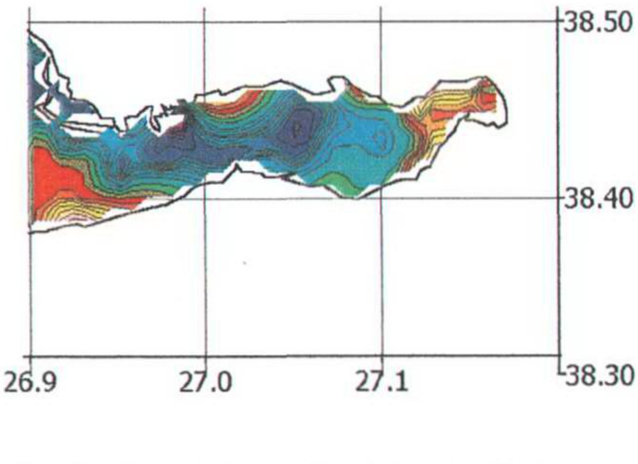

Figure 5.4 The distributions of (a) *in situ* chlorophyll-a concentrations in Izmir Bay and (b) the chlorophyll-a concentrations which were retrieved from NOAA images for the inner bay (November 1997)

(a)

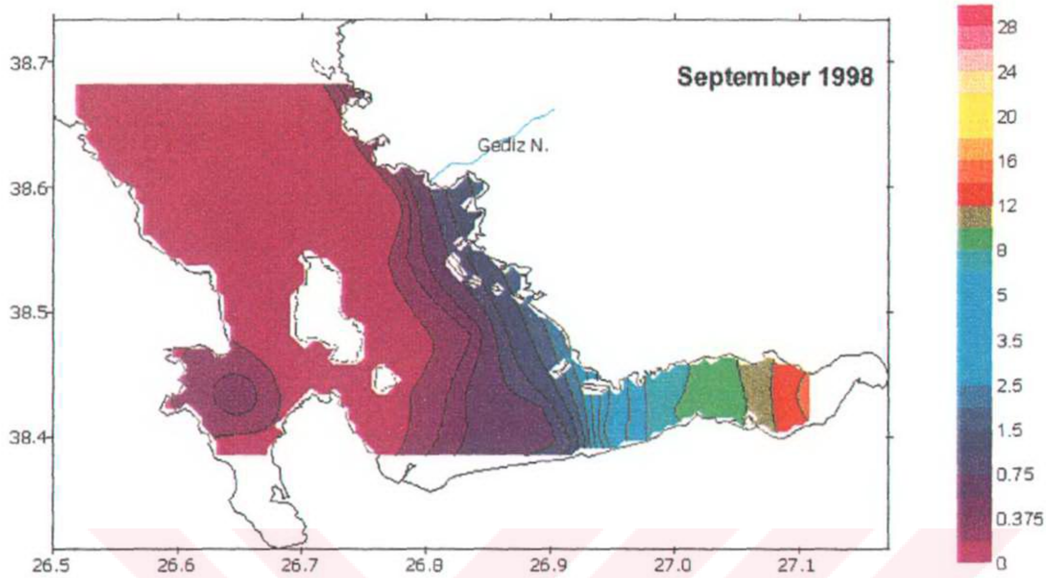

(b)

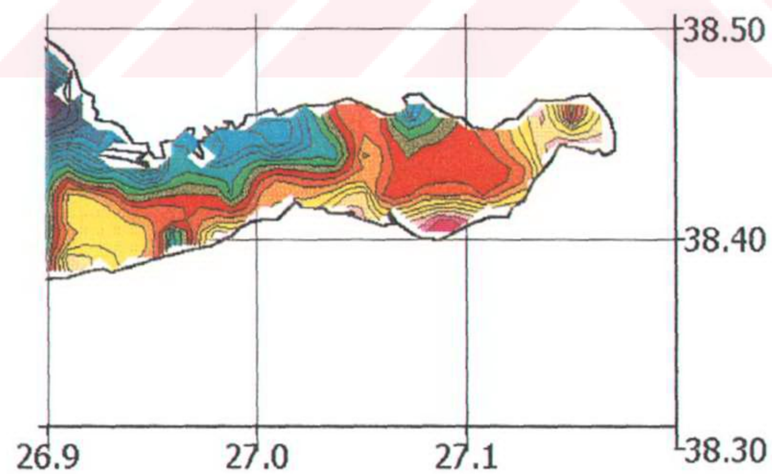

Figure 5.5 The distributions of (a) *in situ* chlorophyll-a concentrations in Izmir Bay and (b) the chlorophyll-a concentrations, which were retrieved from NOAA images for the inner bay (September 1998)

CHAPTER SIX
DISCUSSION AND CONCLUSIONS

AVHRR was designed primarily for meteorological purposes. In oceanography, the most successful use of the sensor is the determination of sea surface temperatures from thermal bands. This use of AVHRR was foreseen right from the beginning, unlike the other applications. The satellite also has the sensitivity to provide information on sediments and chlorophyll amounts in highly turbid coastal waters like the Izmir Bay. Several authors have examined the patterns of water clarity at turbid estuaries (Stumpf, 1987, 1992, Stumpf & Frayer 1997, Stumpf & Pennock 1989, 1991, Stumpf & Tyler, 1988, Tyler & Stumpf, 1989, Stumpf *et al*, 1999, Woodruff *et al.*, 1999). Stumpf's (1992) algorithm was used to remove atmospheric effects from the selected cloud-free images covering the bay and sea surface reflectance maps were produced.

The sea surface reflectance of Izmir Bay shows a seasonal variation. Turbidity increases during the wintertime due to mixing caused by strong winds and resuspension in the water column. Inner and middle regions of the bay are always highly turbid in both winter and summer. The northern part of the bay has relatively high reflectance in all scenes. In shallow waters, the water leaving radiance has an additional component as the light reflected off the bottom. The depth of water is less than 5 meters in and around this region. This shallowness causes high reflectance levels on the scenes.

The desired products of ocean-color data are the concentrations of the constituents like chlorophyll-a rather than the optical properties. The concentrations can only be assessed indirectly by remote sensing, through the influence of their inherent optical properties on the spectral signature of the light remitted from the water body. The concentration of a constituent of the water body can be calculated either from empirical regressions or from bio-optical models, which are implemented using experimental data on the spectral variations of specific optical properties (IOCCG No. 3, 2000).

Bukata *et al.* (1995) suggests the use of multivariate optimization techniques in conjunction with a priori or directly determined pertinent scattering and absorption cross section spectra to determine the subsurface volume reflectance spectrum into co-existing concentrations of near-surface chlorophyll, suspended sediments, and dissolved organic carbon.

The *in situ* data used in this study were not collected for specific calibration purposes of the remotely sensed images. There were no measurements regarding the inherent optical properties of Izmir Bay to construct any bio-optical model. With the data at hand, chlorophyll-a concentrations were derived from empirical regressions so that the constructed model is specific to the Izmir Bay as the empirical algorithms for Case 2 waters are always regional in scope (IOCCG No. 3, 2000).

The AVHRR imagery reveals new spatial and temporal detail on optical properties of Izmir Bay, for the period of 1996-1998. A significant relationship between reflectance in the red region (580-680 nm) and the chlorophyll-a ($r = -0.85$) is found only for the inner and middle regions of the bay and for chlorophyll concentrations exceeding 4 $mg.m^{-3}$. *In situ* data corresponding to the cloud free image set for this study was limited. The monitoring of Izmir Bay is a continuous activity and monthly *in situ* data have been collected for the years 2000 and 2001 to determine the qualitative and quantitative recovery in Izmir Bay after the commencement of operation of the Municipal Waste Water Treatment Plant in April 2000. However, the HRPT Station on IMST had several breakdowns during this period. Inclusion of additional and concurrent satellite and *in situ* data would better substantiate the relationship.

The AVHRR bands indicate the presence of chlorophyll-a. However, being fairly broad, they will also respond to other pigments. This broad response poses no problem for determining relative variations of pigment quantity in a given scene or in determining differences when chlorophyll-a concentrations are higher than 5 $mg.m^{-3}$ as indicated by Stumpf (1987).

Stumpf & Tyler (1987) note that the per cell density of chlorophyll may alter the reflectance response. For example, certain dinoflagellates tend to have more chlorophyll per cell than some diatoms. For a given chlorophyll concentration, the dinoflagellates will have less surface area to reflect near infrared light. This effect should be examined to determine the need for more than one calibration (Stumpf, 1987).

There is a nonlinear relation between sea surface reflectance and the secchi depth readings (r=0.697) in Izmir Bay. TSS and sea surface reflectance are linearly correlated in the outer bay for chlorophyll-a concentrations less than 5 $mg.m^{-3}$.

Estimating turbidity from satellite may be more accurate than measuring it with a secchi disk. Secchi depth measurements can vary greatly, depending on the operator. A sun angle correction should be made which rarely happens for *in situ* Secchi depth measurements (Stumpf, 1987).

Estimation of the optical properties or the concentrations of chlorophyll-a from satellites has different sources of error. There may be calibration errors in the radiance data measured by the satellite sensor. AVHRR does not have onboard calibration. Post-launch calibration techniques developed for the Pathfinder programme have been applied in this study to minimize this error. There may be errors resulting from the atmospheric correction procedure. The Stumpf's (1992) algorithm is based on the theory that near-infrared radiation is absorbed by the water body and thus all measured near-infrared radiation is originating from Rayleigh and Aerosol scattering in the atmosphere. However if, total suspended solids concentration near the surface is significantly high, this assumption causes an overestimation in the aerosol scattering correction, which is also a problem for Izmir

Bay. To overcome this problem, independent atmospheric correction models such as LOWTRAN or MODTRAN can be used, which require input values of many atmospheric parameters. The main disadvantage of these models is the high cost. Another source of error comes from the differences in the spatial and temporal scales of *in situ* and satellite observations. The properties of coastal waters vary greatly over time and space. The *in situ* data should be taken as close as possible to the exact time of the over-flight. In this study the cloud free images were selected for the dates exactly matching the *in situ* measurement ones. AVHRR images were taken around noon but the in situ data collection covers the whole day so there may be differences of several hours. The spectral resolution of AVHRR is 1.1 km, which may bring errors to the correlations with the point samples. The use of *Nv-shuttle* of IMST in future will help to collect better calibration and validation data.

In both Case 1 and Case 2 waters, there is keen interest in predicting primary production and in generating a variety of ancillary products from ocean-colour data. Standard algorithms for estimating water-column primary production using photosynthesis-irradiance relationships rely on remotely sensed chlorophyll-a, light attenuation and estimated surface irradiance. In Case 1 waters, light attenuation in the water column can be approximated reasonably well as a function of chlorophyll-a concentration. In Case 2 waters, on the other hand, the computation of light attenuation will have to account for the role of suspended sediments and dissolved organic matter as well (IOCCG No. 3, 2000).

The studies carried out in Izmir Bay regarding the phytoplankton composition and primary production show that the succession of phytoplankton species is very dynamic and interannual variability is so high in Izmir Bay. It is not possible to end up with a robust conclusion without the validation of estimated PP from empirical algorithms with in situ ^{14}C measurements.

In this study, primary production calculations were also carried out using the empirical approaches developed by Eppley et al. (1985) and Ryther & Yentsch (1957) as stated in Section 1.8. The regression equation given by Eppley et al. (1985) was selected as it is the simplest case and the method of Ryther & Yentsch (1957) was selected as there was a previous study on the primary productivity of Izmir Bay-, which was performed by Balcı et al. (1995) with the same method. As an initial estimate, Ryther and Yentsch (1957) assigned P^{b}_{opt} a constant value of 3.7 mgC (mgChl) $^{-1}$ h^{-1}, which Cullen (1990) suggested should be revised to 4.8 mgC (mgChl) $^{-1}$ h^{-1} due to improvements in the determination of pigment concentrations (Behrenfeld & Falkowski, 1997). So PP estimation from the method of Ryther & Yentsch (1957) for Izmir Bay was carried out both by taking P^{b}_{op} as 3.7 mgC (mgChl) $^{-1}$ h^{-1}, and by taking P^{b}_{op} as 4.8 mgC (mgChl) $^{-1}$ h^{-1}.

There were also primary production measurements, which were based on light/dark bottle method performed by the scientists of Department of Hydrobiology of Ege University Water Products Faculty within the "Monitoring of the Izmir Bay Programme". The values of chlorophyll-a concentrations measured by those scientists were quite different than the *in situ* data of IMST. Also there were great differences between the primary production calculations from the two empirical approaches. This shows that the result of any desired product varies in accordance with the applied methodology. Also the derived relationships from the empirical approaches are valid only for data having statistical properties identical to those of the data set used for the determination of the coefficients. These algorithms are thus particularly sensitive to changes in the composition of water constituents (e.g. regional and seasonal effects) (IOCCG No. 3, 2000). Chlorophyll-a concentrations that were predicted from the AVHRR images were used in the equations given by Eppley *et al.* (1985) and Ryther & Yentsch (1957) for the remotely estimation of primary production in Izmir Bay. Balcı *et al.* (1995) estimated primary production in Izmir Bay by the method of Ryther & Yentsch, (1957), and found that the primary production in the inner bay was between 135-1455 (mgC/m^2/day) for the period of February, 1990-December, 1992. In this study, the primary production amounts that have been estimated by the same method vary from 410.82 to 1986.71 (mgC/m^2/day).

The experimental errors in the field measurements are difficult to evaluate within the present work because the information concerning the accuracy of the measurement protocols for the various datasets used were not available. The spatial resolution of AVHRR is 1.1 km. Thus the sea surface reflection derived from AVHRR will represent an average value over this area. So errors may come from the comparison of chlorophyll-a predicted from satellite with the in situ measured ones if there are great variations in chlorophyll-a (or in apparent and inherent optical properties of water) throughout the field of view. With the model developed in this study to predicted chlorophyll-a values in Izmir Bay, 47% of the variance in the data was explained at the 95% confidence level. When the data of 8.12.1997 was extracted from the analysis, 77% of the variance was explained. The remaining variance which was not explained by the model may be due to errors coming from point measurements versus pixel averages or due to errors in deriving sea surface reflectances from AVHRR.

Collection of *in situ* primary production data in future may help to derive an empirical equation for the Izmir Bay.

While individual scenes can permit examination of specific events, the AVHRR provides sufficient data to look at monthly, seasonal and annual trends in water clarity. The imagery has the potential to describe average conditions in order to determine representative nature of data collected by field programs. The nearly daily imagery may allow us to examine questions relating algal blooms to turbidity – for example, looking at the links between resuspension events, which may bring nutrients into the water column, and the occurrence of algal blooms. While the launch of new sensors, such as the ocean color temperature sensor (OCTS) and the Sea Wide Field Sensor (SeaWiFS), will offer substantially increased capabilities for looking at algal blooms and light attenuation, these sensors can not look at past conditions (Stumpf & Frayer, 1997).

In the case of Izmir Bay, documentation of current and past conditions are essential to understand the variability and change in the system that will affect management strategies. The AVHRR can provide data on large estuaries and turbid coastal systems over a 15 year time period. Combination of AVHRR datasets with new sensors will provide an important description of these systems. Different estuaries may be compared and time series can be developed.

REFERENCES

Akyarlı, A., Uslu, O., Saner, E., & Üçüncüoğlu, E. (1997). An Integrated Approach for Natural Resource Management in the Izmir Bay, Proceedings of the Third International Conference on the Mediterranean Coastal Environment. E. Ozhan (Ed.) Quawra, Malta, November, 1997. 1, 547-561.

Balcı, A., Küçüksezgin, F., Kontaş, A., & Altay, O. (1995). Eutrophication in Izmir Bay, Eastern Aegean. Toxicological and Environmental Chemistry. 48:31-48.

Behrenfeld, M.J., & Falkowski, P.G. (1997). A consumer's guide to phytoplankton primary productivity models, Limnology and Oceanography, 42-7, 1479-1491.

Bizsel, N. & Uslu, O. (2000). Phosphate, nitrogen and iron enrichment in the polluted Izmir Bay, Aegean Sea, Marine Environmental Research, 49,101-122.

Bizsel, N., Benli, H.A., Bizsel, K.C., & Metin, G. (2001). A synoptic study on the phosphate and phytoplankton relationship in the hypereutrophicated Izmir Bay (Aegean Sea), Turk. J. Engin. Environ. Sci., 25, 89-99.

Bizsel, N., Öztürk, M., & Metin, G. (1997). The role of iron on the phytoplankton growth in heavily polluted Izmir Bay, Aegean Sea, Proceedings of the 4th International Conference on Water Pollution, Southampton, UK, Computational Mechanics Publications, 659-669.

Bukata, R.P., Jerome, J.H., Kondratyev, K.Ya., & Pozdnyakov, D.V. (1995). Optical Properties and Remote Sensing of Inland and Coastal Waters. New York: CRC Press, Inc.

Büyükışık, B., Gökpınar, Ş., & Parlak, H. (1997), Ecological Modelling of Izmir Bay, Journal of Fisheries and Aquatic Sciences, 14/1-2, 71-91.

Cracknell, A.P. (1997). The Advanced Very High Resolution Radiometer (AVHRR). London: Taylor and Francis Ltd.

Cracknell, A.P. (1999). Remote sensing techniques in estuaries and coastal zones-an update, Int. J. of Remote Sensing, 20-3, 485-496.

Eppley, R.W., Stewart, E., Abbott, M.R., & Heyman, U. (1985). Estimating Ocean Primary Production from Satellite chlorophyll. Introduction to Regional Differences and Statistics for the Southern California Bight. Journal of Plankton Research. 7-1. 57-70.

Falkowski, P.G., Behrenfeld, M.J., Esaias, W.E., Balch, W., Campbell, J.W., Iverson, R.L., Kiefer, D.A., Morel, A., & Yoder, J.A. (1998). Satellite Primary Productivity Data and Algorithm Development: A Science Plan for Mission to Planet Earth. NASA Tech. Memo. 1998-104566. 42. S.B. Hooker and E.R. Firestone, Eds. NASA Goddard Space Flight Center. Greenbelt, Maryland.

Gieskes, W.W.C. (1991). Particle Analysis in Oceanography, NATO ASI Series, Vol. 627. S. Demers (Ed), Algal Pigment Finger prints: Clue to Taxonspecific Abundance, Productivity and Degradation of Phytoplankton In Seas and Oceans. Berlin: Springer-Werlag. 61-99.

Groupment pour le développement de la Télédétection Aérospatiale - GDTA. (1992). Booklet B1-Physical Bases in Remote Sensing. Toulouse-France: Alberte Fischer.

Hoepffner, N., Sturm, B., Finenko, Z., & Larkin, D. (1999). Depth-integrated primary production in the eastern tropical and subtropical North Atlantic basin from ocean color imagery, Int.J. Remote Sensing, 20-7, 1435-1456.

International Ocean-Colour Coordinating Group. (2000). IOCCG Report Number 3, Remote Sensing of Ocean Colour in Coastal, and Other Optically Complex, Waters. Canada: S. Sathyendranath (Ed.), No. 3, Jerlov, N.G. (1976). Marine Optics. New York: Elsevier.

Lillesand, T.M., & Kiefer, R.W. (1994). Remote Sensing and Image Interpretation. (2nd ed.). New York: John Wiley & Sons.

Lynch, M.J. (September 11-22, 2000). Basic Radiometric Quantities and Definitions. Course Notes for Ocean Color Remote Sensing Course. Erdemli, Turkey

Marine Researches in Izmir Bay. (1998). Dokuz Eylül University Institute of Marine Sciences and Technology. Izmir.

Metin, G. & Cirik, Ş. (1999). Quantitative changes in phytoplankton of Izmir Bay, Journal of Fisheries and Aquatic Sciences, 16/3-4, 363-374.

Parsons, T.R., Takahashi, M., & Hargrave, B. (1990). Biological Oceanographic Processes (3rd ed.). Oxford: Pergamon.

Rao, C.R.N., & Chen, J. (1996). Post launch calibration of the visible and near-infrared channels of the Advanced Very High Resolution Radiometer on the NOAA-14 spacecraft. International Journal of Remote Sensing, 17: 2743-2747.

Robinson, I.S. (1997). Satellite Oceanography: An Introduction for Oceanographers and Remote Sensing Scientists. New York: John Wiley & Sons.

Ryther, J.H., & Yentsch, C.S. (1957). The Estimation of Phytoplankton Production in the Ocean from Chlorophyll and Light Data. Limnology and Oceanography, 2, 281-286.

Strickland, J.D.H. & Parsons, T.R. (1972). A Practical Handbook of Seawater Analysis. (2nd ed.). Bulletin 167. Fisheries Research Board of Canada. Ottawa.

Stumpf, R.P. & Frayer, M.L. (1997). Monitoring Algal Blooms: New Techniques for Detecting Large-Scale Environmental Change. M. Kahru & C.W.Brown (Eds.).

Use of AVHRR Imagery to Examine Long-Term Trends in Water Clarity in Coastal Estuaries: Example Florida Bay.

Stumpf, R.P. & Pennock, J.R. (1989). Calibration of General Optical Equation for Remote Sensing of Suspended Sediments in a Moderately Turbid Estuary. Journal of Geophysical Research. 94(C10): 14,363-14,371.

Stumpf, R.P. & Pennock, J.R. (1991). Remote Estimation of the Diffuse attenuation Coefficient in a Moderately Turbid Estuary. Remote Sensing of Environment. 38: 183-191.

Stumpf, R.P. & Tyler, M.A. (1987). Satellite Detection of Bloom and Pigment Distributions in Estuaries. Remote Sensing of Environment.24: 385-404.

Stumpf, R.P. (1987). Application of AVHRR Satellite Data to the Study of Sediment and Chlorophyll in Turbid Coastal Water. NOAA Technical Memorandum NESDIS AISC 7. Washington D.C.

Stumpf, R.P. (1992). Remote Sensing of Water Clarity and Suspended Sediments in Coastal Waters. Proceedings of the First Thematic Conference on Remote Sensing for Marine and Coastal Environments, New Orleans. SPIE 1930, 293-306.

The Open University. (1997). Seawater: Its Composition, Properties and Behavior. (2nd ed.). Oxford: Butterworth-Heinemann.

Woodruff, D.L., Stumpf, R.P., cope, J.A., & Paerl H.W. (1999). Remote Estimation of Water Clarity in Optically Complex Estuarine Waters. Remote Sensing of Environment. 68: 41-52.